JOURNAL OF PETROLOGY

Journal of Petrology, 2021, Vol. 62, No. 12, 1–19
https://doi.org/10.1093/petrology/egab090
Advance Access Publication Date: 27 October 2021
Original Manuscript

OXFORD

Characterising the Distinct Crustal Protoliths of Roberts Victor Type I and II Eclogites

Matthew F. Hardman[1,2,*], Thomas Stachel[1], D. Graham Pearson[1], Erick J. Cano[3], Richard A. Stern[1], and Zachary D. Sharp[3]

[1]Department of Earth and Atmospheric Sciences, University of Alberta, Edmonton, Canada, T6G 2E3 [2]Gemological Institute of America, Carlsbad, California, USA, 92008 and [3]Department of Earth and Planetary Sciences, University of New Mexico, Albuquerque, USA, 87131

*Corresponding author: E-mail: mhardman@ualberta.ca

Received 22 October 2020; Revised 7 October 2021; Accepted 19 October 2021

Abstract

The origin of the eclogites that reside in cratonic mantle roots has long been debated. In the classic Roberts Victor kimberlite locality in South Africa, the strongly contrasting textural and geochemical features of two types of eclogites have led to different genetic models. We studied a new suite of 63 eclogite xenoliths from the former Roberts Victor Mine. In addition to major- and trace-element compositions for all new samples, we determined $^{18}O/^{16}O$ for garnet from 34eclogites. Based on geochemical and textural characteristics we identify a large suite of Type I eclogites ($n = 53$) consistent with previous interpretations that these rocks originate from metamorphosed basaltic-picritic lavas or gabbroic cumulates from oceanic crust, crystallised from melts of depleted mid-ocean ridge basalt (MORB) mantle. We identify a smaller set of Type II eclogites ($n = 10$) based on geochemical and textural similarity to eclogites in published literature. We infer their range to very low $\delta^{18}O$ values combined with their varied, often very low zirconium-hafnium (Zr-Hf) ratios and light rare earth element-depleted nature to indicate a protolith origin via low-pressure clinopyroxene-bearing oceanic cumulates formed from melts that were more depleted in incompatible elements than N-MORB. These compositions are indicative of derivation from a residual mantle source that experienced preferential extraction of incompatible elements and fractionation of Zr/Hf during previous melting.

Key words: eclogite; oxygen isotopes; subcratonic mantle; subduction; oceanic crust

INTRODUCTION

Mantle eclogite

Eclogite is a high pressure and temperature metamorphic rock with a basaltic to picritic composition, formed in the deep crust or upper mantle (Desmons and Smulikowski 2007). Eclogite *sensu stricto* is comprised of garnet and omphacite—a clinopyroxene that contains between 20% and 80 mol% jadeite ($NaAlSi_2O_6$)—that together comprise ≥75% of the rock, but not individually more than 75% (Clark & Papike, 1968; Desmons & Smulikowski, 2007). Omphacite distinguishes eclogite from other plagioclase-free garnet-clinopyroxene-rich mantle rocks, such as garnet-pyroxenites.

The origin of cratonic mantle eclogites, transported to Earth's surface as xenoliths by kimberlites, has been the focus of an enduring controversy. One hypothesis is that eclogites are the products of crystallisation deep in the mantle from primary mantle-derived melts (e.g. O'Hara & Yoder, 1967; Hatton, 1978; Smyth *et al.*, 1989; Caporuscio & Smyth, 1990). However, there is a strong case against this model, as olivine should be a primary liquidus phase for mantle melts at high pressures (Green & Ringwood, 1967; Jacob, 2004), and the clinopyroxene that crystallises at high pressures has a low jadeite component (Pearson & Nixon, 1996). Alternatively, mantle eclogites may have formed from deeply-subducted and metamorphosed oceanic crust (e.g. Green & Ringwood, 1972; Helmstaedt & Doig, 1975; Helmstaedt & Schulze, 1989). The broadly basaltic to picritic bulk major- and trace-element compositions of many cratonic eclogite xenoliths are similar to mid-ocean ridge basalt (MORB), which forms by extensive adiabatic decompression melting to relatively low pressures (McDonough, 1991; Jacob, 2004). Globally, some cratonic eclogites have more mafic compositions that may indicate protoliths that formed from low-pressure mantle melts in the Archean when mantle potential temperatures were higher (e.g. Jacob & Foley, 1999; Labrosse & Jaupart, 2007; Herzberg *et al.*, 2010).

In addition, many mantle eclogites have positive Eu-anomalies that indicate plagioclase-bearing protoliths, such as those that occur in the intrusive sections of oceanic crust (i.e. gabbros and troctolites; Jacob, 2004; Shu *et al*., 2016). Many mantle eclogite suites have oxygen isotope values ($\delta^{18}O$) significantly outside the range for mantle peridotite ($\delta^{18}O = 5.5 \pm 0.4‰$; Mattey *et al*., 1994; Jacob, 2004; Korolev *et al*., 2018). The $\delta^{18}O$ values of mantle eclogites are, however, within the range of $\delta^{18}O$ values reported for some ophiolite crustal sequences, a range considered to have developed due to hydrothermal alteration of oceanic crust by seawater (Muehlenbachs & Clayton, 1972a, 1972b; Gregory & Taylor, 1981; Ickert *et al*., 2013). This combined evidence favours that mantle eclogites have oceanic crust protoliths that formed at low pressure and then were subducted. Modern-style plate tectonics, including oceanic crust subduction, has been reported to have started at least ~3Ga (Shirey & Richardson, 2011; Windley *et al*., 2021) and possibly as early as the Early Archean (Shu *et al*., 2016).

However, mantle eclogites commonly display evidence that they experienced multistage histories including partial melting during subduction (including the possible loss of tonalite-trondhjemite-granodiorite-type melts; Ireland *et al*., 1994). Mantle eclogites may have also experienced metasomatism by fluids or melts in the mantle, possibly including kimberlite-related metasomatism (Huang *et al*., 2012). This metasomatism may enrich the eclogite in incompatible elements, induce sample recrystallisation, or introduce metasomatic minerals (Dawson, 1984; Gréau *et al*., 2011; Huang *et al*., 2012; Aulbach *et al*., 2020).

Eclogites and the Roberts Victor mine

Eclogite is inferred to comprise only a minor proportion of the subcratonic mantle globally (< 1to 5%; Dawson & Stephens, 1975; Schulze, 1989), but is locally abundant at the former Roberts Victor diamond mine, South Africa (> 90%; Gréau *et al*., 2011). Roberts Victor is located directly on the Colesberg lineament, which marks the collision of the Kimberley and Witwatersrand blocks terminating ~2.88 to 2.94Ga (Schmitz *et al*., 2004; Shirey *et al*., 2004 and references therein).

The eclogite xenoliths from Roberts Victor were initially classified by texture into Groups I and II (MacGregor & Carter, 1970), with the latter inferred to comprise <10% (Gréau *et al*., 2011). MacGregor & Carter (1970) described the Group I eclogites as having subhedral garnets within a clinopyroxene 'matrix', and were later described as having textural features consistent with textural disequilibrium, as well as metasomatism-related recrystallized microstructures (Gréau *et al*., 2011). Group II eclogites were initially defined by interlocking mineral grains and a comparatively 'fresh' appearance (MacGregor & Carter, 1970), considered the more texturally-equilibrated and less metasomatised (Gréau *et al*., 2011). Group I eclogites also have higher average Na_2O_{grt} and K_2O_{cpx} contents than Group II eclogites (McCandless & Gurney, 1989), as well as an offset distribution of $\delta^{18}O$ values generally higher than Group II eclogites (MacGregor & Manton, 1986). Improved and varied analytical methodologies have expanded the distinguishing criteria to include, among others, radiogenic isotope and trace-element compositions (Table 1; see summaries in Gréau *et al*., 2011 and Huang *et al*., 2016). The most recent classification of Roberts Victor eclogite xenoliths classifies them broadly as Types I and II (Gréau *et al*., 2011), corresponding to the original Group I and II eclogites of MacGregor & Carter (1970), respectively, combined with compositional and isotopic compositions—we adopt the updated classification in this study.

Early studies inferred that the Roberts Victor Type II eclogites formed as high pressure cumulates and the Type I eclogites from the remaining liquids (MacGregor & Carter, 1970; Garlick *et al*., 1971). The interpretation that Roberts Victor eclogites have oceanic crustal protoliths later achieved wider acceptance (e.g. Jagoutz *et al*., 1984; MacGregor & Manton, 1986). Since then, Type I eclogites have been inferred as the products of mantle metasomatism, and Type II eclogites as comparatively un-metasomatised, based on their textures and elemental and isotopic compositions (Gréau *et al*., 2011; Huang *et al*., 2012). Subsequent studies have attributed the range of elemental compositions and oxygen isotope compositions of the Type I and II eclogites to lithological variations within protolithic oceanic crust—including oceanic lavas and cumulates—formed at low pressures and subsequently recycled, with possible modification of elemental compositions by partial melting and/or metasomatism (e.g. Radu *et al*., 2019). Due to the complexity of the Roberts Victor eclogite suite, in this study we consolidate new and published literature data to present a new interpretation for the formation of the Type II eclogites at Roberts Victor.

SAMPLE SET AND PETROGRAPHY

In this study we analysed 63 new eclogite xenoliths from Roberts Victor, South Africa, ranging up to 3 cm in maximum dimension. Garnet and omphacite modes generally range between 35 to 65% for the new eclogites in this study, though Aulbach & Jacob (2016) noted that small xenolith size and the coarse-grained nature of many cratonic eclogites means that mode estimates may vary by up to ~10%. On this basis, and since some eclogites may represent small portions of larger mineralogically heterogeneous samples, we restrict the sample set to those rocks that contain ≥75% combined garnet and omphacite even if the abundance of either is individually greater than the 75% cut-off defined by Desmons & Smulikowski (2007). Additional petrographic descriptions for all new eclogites in this study are provided in Supplementary Online Data Appendix 1.

We classify the new eclogites in this study as Type I ($n = 53$) or II ($n = 10$) based on sample texture (Group I and II textures, respectively, after MacGregor & Carter, 1970). The majority of the new Type I eclogites are bimineralic ($n = 43$) though some contain <1% accessory kyanite ($n = 3$), quartz/coesite ($n = 2$), rutile ($n = 3$), sanidine ($n = 1$), and co-existing rutile and sanidine ($n = 1$; Table 2). Accessory mica (< 1%) occurs in 14 Type I eclogites. A primary or secondary origin of these accessory minerals cannot be determined as they were observed only upon sample crushing. The Type I eclogites in this study are comprised of garnet and omphacite grains up to 1 cm in size. In hand specimen, garnet ranges from light to dark orange and omphacite generally from pale to dark green. Omphacite in three kyanite-bearing eclogites is heavily altered and pale grey-green. Omphacite is typically anhedral while garnets are subrounded and commonly occur within a 'matrix' of omphacite. Grain boundaries are commonly irregular rather than polygonal. Some garnet and omphacite grains contain small micro-inclusions with undetermined compositions.

Of the Type II eclogites in this study ($n = 10$) nine are bimineralic and one contains <1% accessory quartz/coesite. The Type II eclogites are coarse-grained with garnet and omphacite up to 1 cm in size. In hand specimen, garnet ranges from light to dark orange and omphacite from pale to dark green. Unlike the Type I eclogites the garnet and omphacite grains typically are subhedral and interlock with straight, moderately polygonal grain boundaries (Fig. 1a). Omphacite

Table 1: Compilation of petrographic and geochemical characteristics of Type I and II eclogites from Roberts Victor, from published literature

		Type I eclogites	Type II eclogites
Texture			
	Grain shape	Subrounded garnets within a matrix of interstitial clinopyroxene	Subhedral garnet and clinopyroxene with equilibrium-type textures: straight interlocking grain boundaries, ~ 120° triple junctions
	Fluid inclusions, melt pockets	Fluid inclusions or melt pockets in minerals occasionally reported	Fluid inclusions or melt pockets in minerals not reported
	Mineral exsolution	Uncommonly reported	Garnet or kyanite may occur as exsolutions in clinopyroxene. Clinopyroxene may occasionally occur as an exsolution in garnet. Rutile exsolutions in garnet and clinopyroxene are commonly reported
Accessory minerals			
	Diamond	Diamond occasionally reported	Diamond not reported
	Rutile	Occasionally reported as accessory phase. Rutile exsolutions in garnet or clinopyroxene not reported	Not reported as accessory phase. Reported as exsolutions (typically needles) in garnet and clinopyroxene
	Phlogopite	Primary phlogopite occasionally reported	No primary phlogopite reported
	Additional accessory phases	Reasonably common Include coesite, rutile, kyanite, sanidine	Rare Include corundum, kyanite, coesite
Elemental chemistry			
	Major- and minor-elements	Na_2O-in-garnet ≥0.07 wt% K_2O-in-clinopyroxene ≥0.08 wt%	Na_2O-in-garnet <0.07 wt% K_2O-in-clinopyroxene <0.08 wt%
	Trace-elements	Higher whole-rock LREE, HFSE, and LILE contents than Type II eclogites	Lower whole-rock LREE, HFSE, and LILE contents than Type I eclogites
Oxygen isotope values			
	$\delta^{18}O$ (garnet)	5.0 to 9.1 ‰	1.1 to 6.6 ‰
Equilibration conditions			
	Temperature range (°C)	897 to 1297°C	811 to 1313°C
	Pressure range (kbar)	39.7 to 64.8 kbar	34.4 to 65.8 kbar

Data sources: This study; MacGregor & Carter (1970); Garlick *et al*. (1971); McCandless & Gurney (1989); Jacob *et al*. (2005); Gréau *et al*. (2011); Huang *et al*. (2012); Huang *et al*. (2016); Radu *et al*. (2019)

commonly has a 'spongy' texture, primarily on its edges, where it may occur locally as a mixture of diopside and plagioclase, possibly related to omphacite destabilisation during xenolith eruption (Gréau *et al*., 2011, and references therein). Garnet and omphacite lack the small unidentified micro-inclusions observed in some minerals in Type I eclogites. Instead, garnet and omphacite grains tend to contain a low abundance (< 1 vol %) of rutile needles which are commonly locally oriented, sometimes with multiple directions that intersect one another (Fig. 1). Garnet occurs extremely rarely as an inclusion in omphacite, either as small (< 500 μm) sub-rounded, irregular elongate inclusions (Fig. 1b), or thin, < 5 μm wide and ≤ 80 μm long inclusions (Fig. 1c). Orthopyroxene exsolution lamellae occur in omphacite grains in samples RV-27 and RV-62. Fine-grained (< 150 μm diameter) rutile, amphibole, and spinel occur along grain boundaries in all Type II eclogites. The inter-granular rutile grains commonly have thin ilmenite rims (< 20 μm thick) and ilmenite exsolution lamellae (Fig. 1d). The inter-granular mineral assemblages in these samples are inferred to be secondary.

ANALYTICAL METHODS

Major-element compositions

Garnet and omphacite grains were analysed for their major-element compositions using a JEOL 8900R Electron Probe Microanalyser at the University of Alberta. Grains from all samples were analysed in grain mounts, and grains from nine Type II eclogites were also analysed in thin section. Most grains were analysed with a 2 μm focused beam with 20 kV accelerating voltage and 20 nA current. Peak count times were 30 s for Mg, Ca, Ti, Cr, Mn, and Fe, 40 s for Al and Si, and 60 s for Na, with equal time spent analysing total background. Lower limits of detection (LLD) as oxide wt% are 0.05 wt% for Nb_2O_5 and between 0.01 and 0.03 wt% for all other elements (Supplementary Online Data Appendix 2). A subset of garnet and omphacite were re-analysed using modified analytical conditions, including different on-peak count times, and a 20 μm beam operated at 20 kV and 50 nA. Additional details, including the LLD for data acquired using the modified conditions, are given in Supplementary Online Data Appendix 2.

Trace-element compositions

Trace-element compositions (REE, Sr, Zr, Y, Nb, Ba, and Hf) were determined at the Arctic Resources Lab (ARL), University of Alberta, for the same garnet and omphacite grains using a sector-field laser ablation inductively-coupled plasma mass spectrometer (LA-ICP-MS; Element IIXR) coupled with a Resonetics RESOlution M-50 LR 193 nm excimer laser system. Grains were analysed using a 130 μm diameter spot in low mass resolution mode, with a repetition rate of 10 Hz and fluence (at the ablation site) of between 3.5 to 4.0 J/cm^2. Analyses comprised 40 s backgrounds, 60 s on ablation, and 40 s

Table 2: Mineral abundances, group classification, and calculated pressure–temperature conditions for new eclogite xenoliths in this study. All eclogites are classified as Type I, II_L, II_H, or II_{No} using the new classification method in this study. Samples are also classified as IA, IB, IK, IIA, or IIB using the Huang *et al.* (2012) method. Additional petrographic information is provided in Supplementary Online Data Appendix 1

Sample	Type (this study)	Type (Huang *et al.*, 2012)	Grt	Omp	San	Ky	SiO_2	Rut	T (°C)[a]	P (kbar)[a]
RV-1	II_L	IIB	45	55	-	-	-	-	1224	60.2
RV-3	I	IB	50	50	-	-	-	< 1%	1138	54.7
RV-4	II_L	IIB	40	60	-	-	-	-	1054	49.4
RV-5	I	IB	50	50	-	-	-	-	1197	58.4
RV-6	I	IA	40	60	-	-	-	-	998	45.9
RV-7	I	IB	40	60	-	-	-	-	1297	64.8
RV-8	I	IB	45	55	-	-	-	-	1251	61.9
RV-9	I	IB	50	50	-	-	-	-	1140	54.9
RV-10	II_L	IIB	45	55	-	-	-	-	1067	50.2
RV-11	I	IB	48	52	-	-	-	-	1148	55.4
RV-12	I	IB	55	45	-	-	-	-	1078	50.9
RV-13	I	IB	55	45	-	-	-	-	1220	59.9
RV-14	II_L	IIB	45	55	-	-	-	-	1107	52.7
RV-15	I	IB	80	20	-	-	-	-	1118	53.4
RV-16	I	IA	40	60	< 1%	-	-	< 1%	1037	48.3
RV-17	I	IB	50	50	-	-	-	-	1075	50.8
RV-18	I	IB	60	40	-	-	-	-	1195	58.3
RV-19	I	IA	40	60	< 1%	-	-	-	1164	56.3
RV-20	II_L	IIA	50	50	-	-	-	-	1094	51.9
RV-21	I	IB	40	60	-	-	-	-	1122	53.7
RV-22	II_L	IIB	40	60	-	-	-	-	1116	53.3
RV-23	I	IB	60	40	-	-	-	-	1247	61.6
RV-24	I	IB	50	50	-	-	-	-	947	42.8
RV-25	I	IB	60	40	-	-	-	-	1091	51.7
RV-26	I	IK	45	55	-	< 1%	-	-	1260	62.5
RV-27	II_H	IIA	40	60	-		< 1%	-	911	40.5
RV-29	I	IK	65	35	-	< 1%	-	-	1248	61.7
RV-30	I	IB	50	50	-	-	-	-	1169	56.6
RV-31	I	IB	40	60	-	-	-	-	1214	59.5
RV-32	I	IB	45	55	-	-	-	-	1113	53.1
RV-33	I	IB	45	55	-	-	-	-	1151	55.5
RV-34	I	IB	40	60	-	-	-	-	1147	55.3
RV-36	I	IB	50	50	-	-	-	-	1163	56.3
RV-37	I	IB	45	55	-	-	-	-	1122	53.7
RV-38	I	IB	50	50	-	-	-	-	1112	53.1
RV-39	I	IB	40	60	-	-	-	< 1%	1181	57.5
RV-40	I	IB	45	55	-	-	-	-	1143	55.0
RV-41	I	IB	60	40	-	-	-	-	1122	53.7
RV-42	I	IB	37	63	-	-	-	-	1121	53.7
RV-43	I	IB	53	47	-	-	-	-	1220	59.9
RV-44	I	IB	50	50	-	-	-	-	1148	55.3
RV-45	I	IB	45	55	-	-	-	-	1158	56.0
RV-46	I	IA	45	55	-	-	-	-	1077	50.9
RV-47	I	IB	47	53	-	-	-	-	1100	52.3
RV-48	I	IB	50	50	-	-	-	-	1106	52.7
RV-49	I	IB	45	55	-	-	-	< 1%	1251	61.9
RV-50	I	IK	35	65	-	< 1%	-	-	1175	57.0
RV-51	I	IB	55	45	-	-	-	-	1159	56.0
RV-52	I	IA	45	55	-	-	-	-	1175	57.0
RV-53	I	IB	45	55	-	-	-	-	1121	53.6
RV-54	II_L	IIB	50	50	-	-	-	-	1275	63.4
RV-55	I	IB	55	45	-	-	-	-	1121	53.6
RV-56	I	IB	50	50	-	-	< 1%	-	1158	56.0
RV-57	I	IA	40	60	-	-	< 1%	-	1145	55.1

Continued

Table 2: Continued

Sample	Type (this study)	Type (Huang *et al.*, 2012)	Grt	Omp	San	Ky	SiO_2	Rut	T (°C)[a]	P (kbar)[a]
RV-58	I	IB	47	53	-	-	-	-	1208	59.2
RV-59	I	IB	50	50	-	-	-	-	1074	50.7
RV-60	II_L	IIA	50	50	-	-	-	-	1176	57.1
RV-61	I	IB	50	50	-	-	-	-	897	39.7
RV-62	II_L	IIB	50	50	-	-	-	-	1116	53.3
RV-63	I	IB	45	55	-	-	-	-	1056	49.5
RV-64	I	IB	45	55	-	-	-	-	1156	55.8
RV-65	I	IB	50	50	-	-	-	-	1085	51.4
RVSA71	I	IB	50	50	-	-	-	-	953	43.2

[a]Temperatures (T) are calculated using the Krogh (1988) thermometer, and pressures (P) by extrapolation to the Hasterok & Chapman (2011) 38 mW/m^2 model geotherm

Abbreviations: Grt = garnet, Ky = kyanite, Omp = omphacite, Rut = rutile, San = sanidine, SiO_2 = quartz/coesite

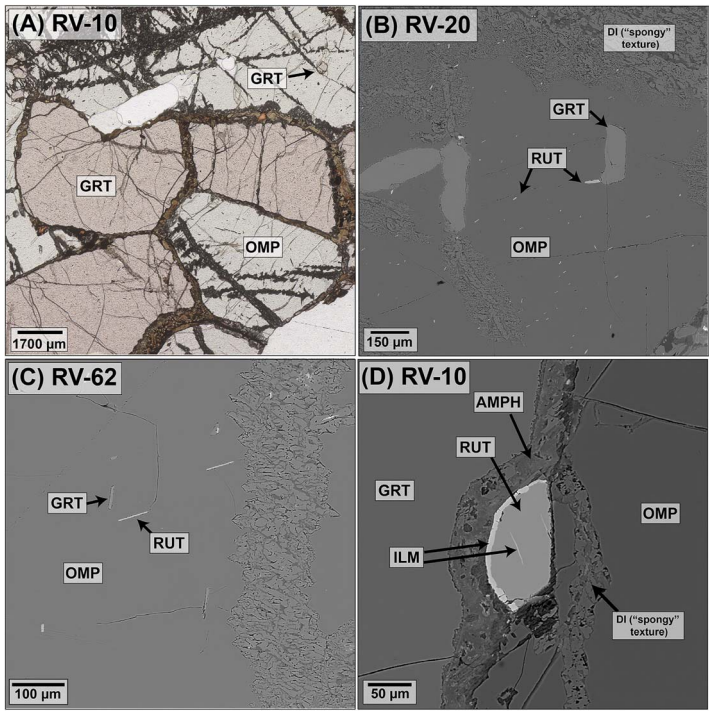

Fig. 1. (a) Plane polarised transmitted light and (b), (c), (d) backscattered electron images of thin sections of select Type II eclogites in this study. Abbreviations: AMPH = amphibole, DI = diopside, GRT = garnet, ILM = ilmenite, OMP = omphacite, RUT = rutile.

post-ablation washout, with helium as the carrier gas. Standard reference material NIST612 glass was used as primary calibration standard with ^{43}Ca as internal standard. ThO/Th was monitored ($< \sim 0.5\%$) to minimise interference from oxide production during analysis. Data were reduced offline using Iolite version 3.32. Garnet PHN3511 was used as a secondary standard to assess long-term repeatability and accuracy for these analyses. An overview of PHN3511 analyses acquired during this study is included in the supplementary material of Hardman *et al.* (2018), incorrectly labelled in that study as PHN3571.

Oxygen isotope compositions

Oxygen isotope ratios ($^{18}O/^{16}O$) were determined for garnets from 34 new eclogite xenoliths via secondary ion mass spectrometry (SIMS) at the Canadian Centre for Isotopic Microanalysis (CCIM), University of Alberta using a Cameca IMS 1280 multi-collector ion microprobe. Detailed analytical methods and the standard reference materials (S0068—Gore Mountain Ca-Mg-Fe garnet and S0088B—grossular garnet) are detailed by Ickert & Stern (2013). All $^{18}O/^{16}O$ ratios are reported in per mil (‰) and expressed in delta notation ($\delta^{18}O$) relative to Vienna Standard Mean Ocean Water (VSMOW; Baertschi, 1976) in equation 1:

$$\delta^{18}O\ (‰) = [(^{18}O/^{16}O)_{sample}/(^{18}O/^{16}O)_{VSMOW}] - 1 \quad (1)$$

The average analytical uncertainty for garnet $\delta^{18}O$ values determined by SIMS in this study is $\pm 0.30‰$ (2σ).

Co-existing garnet and omphacite from eight eclogites in this study were selected for determination of their oxygen isotope compositions ($^{18}O/^{16}O$) by laser fluorination (LF). Ultra-pure mineral

Table 3: Average oxygen isotope compositions ($\delta^{18}O$) for garnet and omphacite from eclogite xenoliths in this study, determined by SIMS and laser fluorination (LF)

Sample	Type	$\delta^{18}O_{grt}$ [a] (SIMS)	$\delta^{18}O_{grt}$ [a] (LF)	$\delta^{18}O_{omp}$ [a] (LF)
RV-1	II_L	2.37	2.609	2.324
RV-3	I	6.13	-	-
RV-6	I	6.83	-	-
RV-7	I	5.68	-	-
RV-9	I	5.73	-	-
RV-10	II_L	2.83	3.015	2.682
RV-11	I	5.72	-	-
RV-13	I	6.04	-	-
RV-16	I	7.13	7.471	6.914
RV-19	I	5.37	5.457	4.843
RV-20	II_L	2.80	2.725	-
RV-21	I	6.60	-	-
RV-22	II_L	1.79	1.673	1.564
RV-24	I	7.59	7.530	7.320
RV-25	I	6.32	-	-
RV-27	II_H	4.60	4.562	4.311
RV-29	I	5.09	-	-
RV-30	I	6.27	-	-
RV-31	I	5.75	-	-
RV-34	I	6.63	-	-
RV-37	I	6.20	-	-
RV-38	I	6.53	-	-
RV-42	I	6.46	-	-
RV-45	I	6.46	-	-
RV-46	I	6.68	-	-
RV-48	I	6.29	-	-
RV-49	I	6.27	-	-
RV-51	I	6.63	-	-
RV-54	II_L	2.27	-	-
RV-56	I	6.34	-	-
RV-58	I	6.61	-	-
RV-59	I	6.77	-	-
RV-61	I	7.10	-	-
RV-62	II_L	2.73	-	-

[a]Calculated using Equation 1

separates were picked by binocular microscope and washed successively in 10 Milli-Q water, 6N HCl, and again in 10 Milli-Q water. Approximately 1 to 2 mg of each mineral was loaded into a 44-well nickel sample plate and their oxygen was extracted via LF at the Center for Stable Isotopes at the University of New Mexico using the standard LF technique of Sharp (1990) modified for high precision. Purified sample O_2 gas was expanded into a Thermo Fisher MAT 253 Isotope Ratio Mass Spectrometer specifically configured to run O_2 gas. Each sample run consisted of 40 iterations, each of which included a 26 s collection time for both the reference and sample gases. All $^{18}O/^{16}O$ ratios are reported in per mil relative to VSMOW. Repeat $\delta^{18}O$ values for garnets in this study determined by LF are within ±0.35‰ of values determined by SIMS (Table 3). See Supplementary Online Data Appendix 2 for additional details.

RESULTS

Major-element compositions

To compare new results with existing data, we have compiled compositional data for 75 Roberts Victor eclogites from published literature. All compiled samples have textural information so that their classification as Type I or II is possible (Table 4 and Supplementary Online Data Appendix 3). Garnets in new Roberts Victor eclogites in this study span a compositional range that overlaps with literature garnet compositions, and include pyrope-, almandine-, and grossular-rich varieties (Fig. 2a; Supplementary Online Data Appendix 4). Garnets from new Type II eclogites have lower average Mg# (0.53; Mg/[Mg + Fe]) but higher average Ca# (0.37; Ca/[Ca + Mg]) than garnets from new Type I eclogites (0.66 and 0.22, respectively). Most of the garnets in the new Type I eclogites have $Na_2O \geq 0.09$ wt% and all garnets from the new Type II eclogites have $Na_2O < 0.09$ wt%, consistent with the findings of McCandless & Gurney (1989).

Clinopyroxenes from the new Roberts Victor eclogites are omphacitic in composition and overlap with omphacite compositions in published literature (Fig. 2b). The quadrilateral-jadeite-aegerine compositions of omphacites from Type I and II eclogites generally overlap. Omphacites from Type II eclogites have slightly lower average Mg# (0.79) and higher Ca# (0.53) than do omphacites from the Type I eclogites (0.83 and 0.47, respectively). Most omphacite in the new Type I eclogites have $K_2O \geq 0.08$ wt% and all of those in the new Type II eclogites have $K_2O < 0.08$ wt%, consistent with McCandless & Gurney (1989).

Table 4: Sources for elemental and isotopic data for eclogites from published literature. All major-element, trace-element, and oxygen isotope data from published literature are given in Supplementary Online Data Appendix 3

Citation	Major-elements	Trace-elements	Oxygen isotope compositions ($^{18}O/^{16}O$)
Caporuscio (1990)	-	-	x
Caporuscio & Smyth (1990)	x	x	-
Garlick *et al*. (1971)	-	-	x
Gréau *et al*. (2011)	x	x	x
Harte & Kirkley (1997)	x	-	-
Hatton (1978)	x	-	-
Huang *et al*. (2012)	x	x	-
Huang *et al*. (2014b)	x	x	-
Huang *et al*. (2016)	-	-	x
Jacob *et al*. (2005)	x	x	x
Jacob *et al*. (2003)	-	x	-
Kiseeva *et al*. (2017)	x	x	-
MacGregor & Manton (1986)	x	x	-
McDade (1999)	-	x	-
Radu *et al*. (2019)	x	x	x

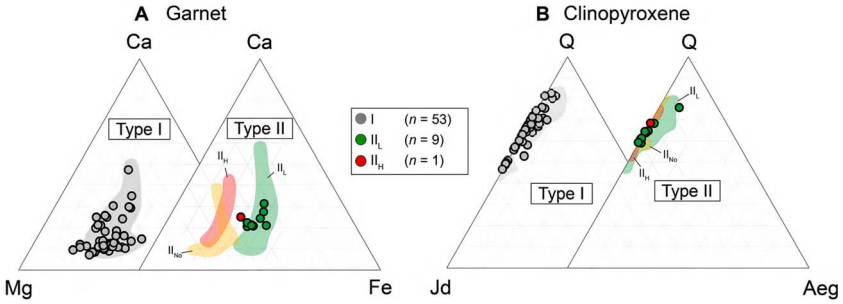

Fig. 2. Major-element compositions of (a) garnets and (b) omphacites from Roberts Victor eclogites in this study ($n = 63$), as well as fields of published literature data ($n = 75$). Data sources are summarised in Table 4 and data from published literature are included in Supplementary Data Electronic Appendix 3. All minerals are divided into Types I, II_{No}, II_L, and II_H using the new classification method in this study (section *Classification of Roberts Victor eclogites*). Garnets are compared by their Mg-Ca-Fe compositions and omphacites by their quadrilateral-jadeite-aegerine (Q-Jd-Aeg) compositions after Morimoto *et al*. (1988).

Trace-element compositions

Garnets from new Type I eclogites are $LREE_N$-depleted with variable $MREE_N$-$HREE_N$ slopes from negative to positive, when normalized to CI chondrite ('$_N$;' McDonough & Sun, 1995; Fig. 3a; Supplementary Online Data Appendix 4). Garnets from most Type II eclogites are more strongly $LREE_N$-depleted and typically characterised by flat to positive $MREE_N$-$HREE_N$ slopes (Fig. 3b). Eu-anomalies ($[Eu/Eu^*]_N$, $Eu^* = 0.5 \times [Sm_N + Gd_N]$) range from negative to positive values for both Type I and II eclogitic garnet. Garnets from new Type II eclogites have higher average Eu-anomalies (1.30) than do those from new Type I eclogites (1.04), though one Type I kyanite-bearing eclogite (RV-26) has the highest Eu-anomaly of all new samples ($Eu/Eu^* = 2.17$). The new Type I and II eclogitic garnet REE compositions overlap with or are slightly outside the range of compositions from published literature (Figs 3a and 3b).

Omphacites from new Type I eclogites are generally $LREE_N$-enriched with negatively sloped REE_N patterns, some with mild relative depletion of the LREE La, Ce, and Pr, indicated by positive slopes from La_N to Nd_N (Fig. 3c; Supplementary Online Data Appendix 4). Omphacites from Type II eclogites have convex-upward REE_N patterns characterised by strong $LREE_N$-depletion with subchondritic La through Nd, and negative $MREE_N$-$HREE_N$ slopes (Fig. 3d). Omphacites from new Type I and II eclogites generally have positive Eu- and Sr-anomalies ($[Sr/Sr^*]_N$, $Sr^* = 0.5 \times [Pr_N + Nd_N]$, normalised to chondrite), while negative Eu- and Sr-anomalies are very uncommon (Figs 3c and 3d; Supplementary Online Data Appendix 4). Omphacites from new Type II eclogites have similar Eu-anomalies (1.15) but higher positive Sr-anomalies (7.55) than new Type I eclogites (1.15 and 3.27, respectively). The REE compositions of omphacite from new Type I and II eclogites are generally within but marginally expand the range of compositions from published literature (Figs 3c and 3d).

Oxygen isotope compositions

Oxygen isotope values ($\delta^{18}O$) determined by SIMS for garnet from 34 new Roberts Victor eclogites range from 1.8 to 7.6‰ (Table 3). The $\delta^{18}O$ for garnets from eight xenoliths determined by laser fluorination are within 0.35‰ of the values for SIMS of garnets from the same samples. The $\delta^{18}O$ of omphacite available for seven xenoliths are within 0.65‰ of their co-existing garnets (Table 3). The $\delta^{18}O$ values of garnets from the new Roberts Victor eclogites are dominantly outside of the canonical mantle range of $\delta^{18}O = 5.5 \pm 0.4$‰ (Mattey *et al*., 1994) and have an approximately bimodal distribution that spans a similar range as whole-rock $\delta^{18}O$ values from the Semail ophiolite, Oman, as well as published values from other Roberts Victor eclogites (Fig. 4). Garnets from new Type II eclogites have $\delta^{18}O$ values that are below the mantle range ($\delta^{18}O = 1.8$ to 2.8‰,

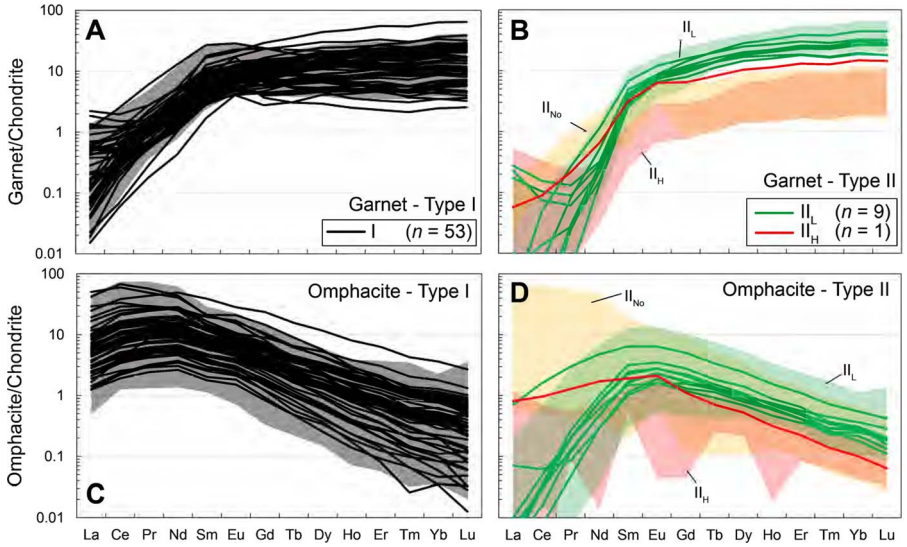

Fig. 3. REE_N patterns for garnets from (a) Type I and (b) Type II eclogites, and omphacites from (c) Type I and (d) Type II Roberts Victor eclogites, normalised to chondrite (McDonough & Sun, 1995). All minerals are subdivided into Type I, II_{No}, II_L, and II_H using the new method in this study (section *Classification of Roberts Victor eclogites*). Solid lines correspond to new eclogites from this study ($n = 63$) and fields correspond to the full range of compositions from published literature ($n = 75$).

$n = 7$), whereas the new Type I eclogitic garnets have a higher range of values that overlaps with and exceeds the canonical mantle range ($\delta^{18}O = 5.1$ to 7.6‰, $n = 27$; Fig. 4). Type I and II eclogites from published literature each have broader $\delta^{18}O$ ranges than the new data (5.0 to 9.1‰, $n = 24$, and 1.1 to 6.6‰, $n = 20$, respectively; Fig. 4; Supplementary Online Data Appendix 3).

Calculated pressure–temperature conditions of last equilibration

Equilibration temperatures and pressures for eclogites in this study and published literature are calculated by projection of Fe-Mg garnet-clinopyroxene exchange temperatures (Krogh, 1988) onto the 38 mW/m^2 model geotherm of Hasterok & Chapman (2011; Table 2; Fig. 5; Supplementary Online Data Appendix 3). The 38 mW/m^2 model geotherm best fits available pressure–temperature data for Roberts Victor (Grütter, 2009 and references therein). The calculated temperatures for new Type I eclogites at Roberts Victor in this study have a temperature and pressure range of 900 to 1300°C and 40 to 65 kbar, respectively (Table 2). These calculated conditions have a slightly wider spread than Roberts Victor eclogites in published literature (950 to 1280°C and 43 to 64 kbar). Type II eclogites in this study have a calculated temperature–pressure range (910 to 1270°C and 41 to 63 kbar, respectively) that is narrower than the range of calculated conditions for published eclogites (810 to 1310°C and 34 to 66 kbar). These ranges exclude two Type II eclogites from published literature with calculated temperatures >1350°C, which exceed the mantle adiabat at lithospheric depths. The thermometry results indicate that Type I and II eclogites are both distributed throughout the lithospheric mantle.

DISCUSSION

Classification of Roberts Victor eclogites

Eclogites at Roberts Victor were initially classified based on sample texture into Groups I and II (MacGregor & Carter, 1970). This textural classification was later shown to correspond to differences in minor-elements (Na_2O-in-garnet, K_2O-in-clinopyroxene; McCandless & Gurney, 1989) and oxygen isotope compositions (MacGregor & Manton, 1986; Table 1). Gréau *et al.* (2011) defined the Type I and II eclogites (with the textures of the original defined Group I and II eclogites, respectively; MacGregor & Carter, 1970) based on their major-element, trace-element, and isotopic compositions. Huang *et al.* (2012) sub-divided Type I eclogites into Type IK (kyanite-bearing), Type IA (bimineralic; garnet FeO > 17 wt%), and Type IB (bimineralic; garnet FeO ≤ 17 wt%), and Type II eclogites into Type IIA (garnet MgO > 12 wt%) and Type IIB (garnet MgO ≤ 12 wt%).

Based on a new compiled eclogite data set that includes 63 new eclogites in this study and 75 additional eclogites from published literature (Table 4; Supplementary Online Data Appendix 3), we revisit the classification of the Type II eclogites at Roberts Victor. We propose a modified classification method that defines the classes Type I, II_L, II_H, and II_{No} using whole-rock chondrite-normalised REE patterns and whole-rock Mg# (Fig. 6). Whole-rock major- and trace-element compositions for all eclogites in this study and published literature are reconstructed using mineral chemistry and modal abundances. When mineral modes are not given in published literature, we assume garnet and omphacite modes of 50% each.

Type I eclogites ($n = 100$ combined from this study and published literature) have a variety of reconstructed whole-rock REE_N patterns generally characterised by superchondritic REE abundances, with occasional subchondritic La and/or Ce (> 0.3x chondrite; Fig. 7). Type I eclogites have negative chondrite-normalised Ti-anomalies ($[Ti/Ti^*]_N$, $Ti^* = 0.5 \times [Eu_N + Dy_N]$) and positive Sr-anomalies (Fig. 8). The Type I eclogites at Roberts Victor are not the principle focus of this study, and so we retain them as Type I without subdivision into Type IA, IB, and IK (Huang *et al.*, 2012), to avoid mixing classification methods based on different criteria.

Type II eclogites compiled in this study ($n = 38$) also have a variety of whole-rock REE_N patterns as well as negative Ti-anomalies and positive Sr-anomalies (Figs 7 and 8). However, 34 of the eclogites with Type II textures are 'LREE-depleted' (whole-rock $Sm_N/Nd_N > 1$)

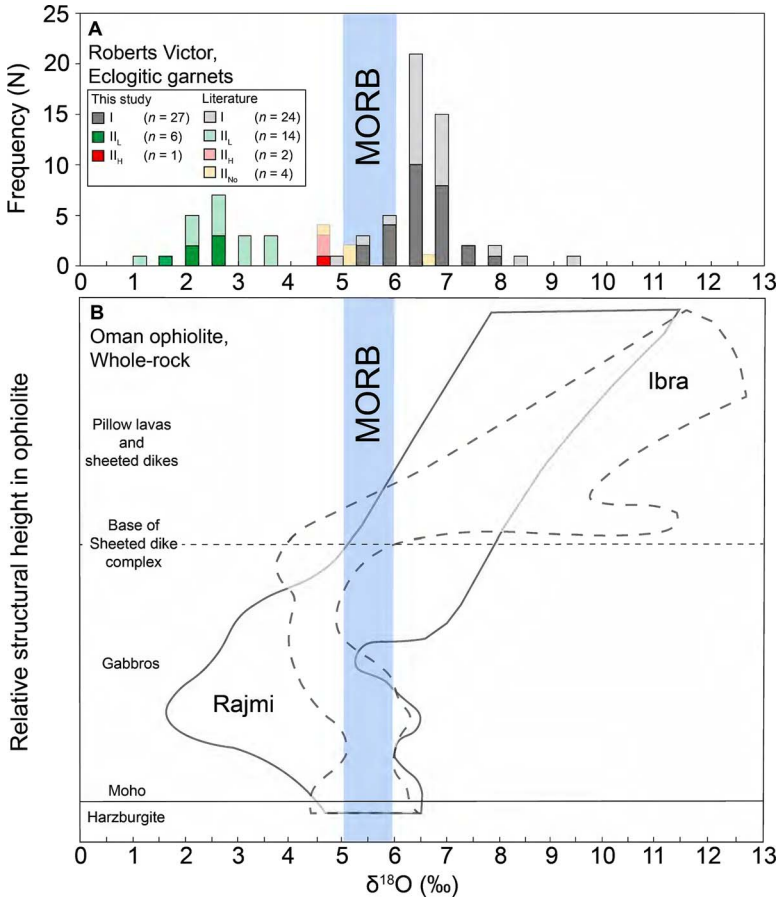

Fig. 4. (a) Frequency distribution of $\delta^{18}O$ for garnets from eclogites at Roberts Victor, from this study ($n = 34$, solid bars) and published literature ($n = 44$, transparent bars; Table 4). Samples are classified into Types I, II_{No}, II_L, and II_H. The range for $\delta^{18}O$ for MORB ($\sim 5.4 \pm 0.3$ ‰; Cano *et al.*, 2020), which is within the canonical mantle range (5.5 ± 0.4 ‰; Mattey *et al.*, 1994), is shown as a pale blue field. (b) Variation in $\delta^{18}O$ values of whole-rock samples from the Oman ophiolite, for the Rajmi and Ibra localities, compared to the inferred MORB range. Figure is adapted from Stakes & Taylor (1992).

with subchondritic LREE (La, Ce, and occasionally Pr, Nd, and Sm) and superchondritic, flat to positively-sloped $MREE_N$-$HREE_N$ ($Lu_N/Gd_N \geq 1$). We classify these eclogites as Type II_L ($n = 29$) if they have whole-rock molar Mg# < 0.70, and Type II_H ($n = 5$) if they have whole-rock molar Mg# ≥ 0.70. The subscripts '$_L$' and '$_H$' correspond to whole-rock Mg# lower than or higher than the chosen Mg# cutoff, respectively. Four additional eclogites with Type II textures have flat or $LREE_N$-enriched whole-rock REE_N patterns ($Sm_N/Nd_N \leq 1$), flat whole-rock $MREE_N$-$HREE_N$ slopes, variable amounts of relative $LREE_N$ enrichment, and occasional positive Eu-anomalies (Fig. 7). We classify these eclogites as Type II_{No} which references their 'non-depleted' whole-rock REE_N patterns.

This new classification departs from the Huang *et al.* (2012) method as we subdivide Type II eclogites using whole-rock compositions, rather than garnet-only, and use a larger eclogite database that includes samples from Huang *et al.* (2012) as well as recent studies (e.g. Radu *et al.*, 2019; Table 4). The basis for using whole-rock REE_N patterns as a classifier is the extreme similarity of REE_N pattern shapes within each of the two subtypes (Type II_L and II_H), as well as distinctly different whole-rock Mg#, with a cut-off of

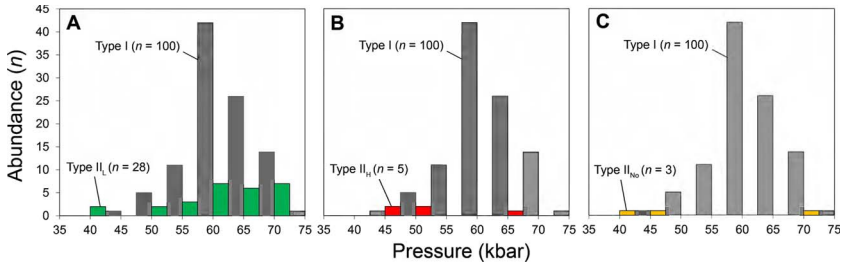

Fig. 5. Frequency distributions of calculated equilibration pressures for eclogites at Roberts Victor, from this study ($n = 63$) and published literature ($n = 73$). Type I eclogites are compared with (a) Type II_L, (b) Type II_H, and (c) Type II_{No} eclogites. One Type II_L and one Type II_{No} eclogite from published literature are not plotted as their calculated pressures exceed the adiabat.

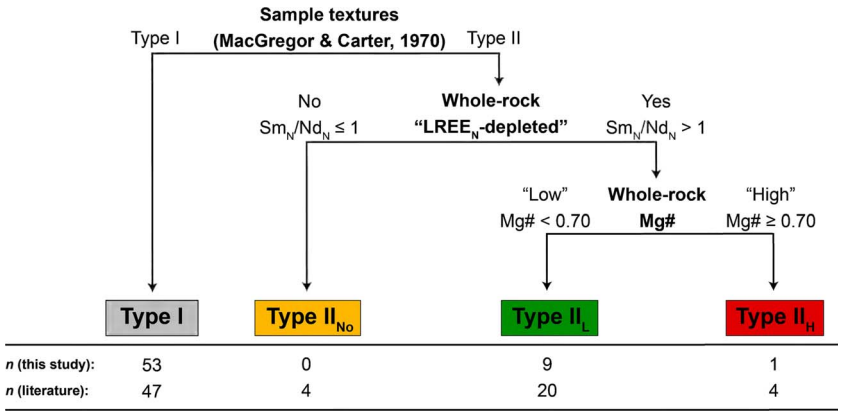

Fig. 6. New classification method for Roberts Victor eclogites. Eclogites in Types I, II_{No}, II_L, and II_H have different whole-rock compositions (section *Classification of Roberts Victor eclogites*). (1) Eclogites are subdivided into Type I or II based on sample texture after MacGregor & Carter (1970). (2) Type II eclogites are subdivided based on whether the whole-rock compositions are 'LREE$_N$-depleted' (normalised to chondrite; McDonough & Sun, 1995). (3) Type II eclogites with 'LREE$_N$-depleted' whole-rock compositions are subdivided further based on their molar Mg# (Mg/[Mg + Fe]). Sample abundances (*n*) from this study and published literature for each group are indicated.

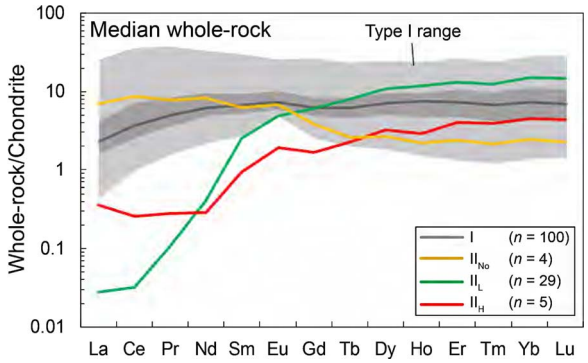

Fig. 7. Reconstructed whole-rock REE$_N$ compositions of Roberts Victor eclogites, normalised to chondrite (McDonough & Sun, 1995). Data are from this study ($n = 63$) and published literature ($n = 75$). Whole-rock compositions are reconstructed based on garnet and clinopyroxene only, using known mineral modes. We apply modes of 50% garnet and 50% omphacite when modes are unavailable. Solid lines are median compositions for Types I, II_{No}, II_L, and II_H eclogites. The light grey field is the full range of Type I eclogite compositions, and the dark grey field is the range of Type I eclogite compositions between the 1st and 3rd quartile.

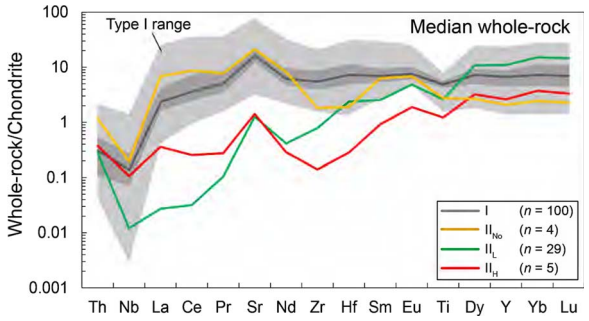

Fig. 8. Reconstructed whole-rock extended trace-element patterns for Roberts Victor eclogites, normalised to chondrite (McDonough & Sun, 1995). Data are from this study ($n = 63$) and published literature ($n = 75$). Whole-rock compositions are reconstructed based on garnet and omphacite only, using known mineral modes. We apply modes of 50% garnet and 50% omphacite when modes are unavailable. Solid lines are median compositions for Types I, II_L, II_H, and II_{No} eclogites. The light grey field is the full range of Type I eclogite compositions, and the dark grey field is the range of Type I eclogite compositions between the 1st and 3rd quartile.

0.70. The use of whole-rock Mg# is similar to the use of garnet MgO contents by Huang *et al.* (2012) but is expected to more accurately reflect igneous processes such as olivine fractionation or accumulation during oceanic crust formation (Perk *et al.*, 2007). Whole-rock Mg# has also been used in recent studies for other classifications of cratonic eclogites (e.g. Aulbach & Jacob, 2016).

Based on the chosen subdivision criteria, Type II_L, II_H, and II_{No} eclogites have several additional compositional characteristics. Garnets from Type II_L and II_H eclogites have offset Mg-Ca-Fe compositions characterised by higher Fe contents in Type II_L eclogitic garnet (Fig. 2a). Garnet and omphacite from Type II_L eclogites have higher ΣREE than Type II_H, as well as smaller positive Eu-anomalies (Figs 3b and 3d). Type II_L and II_H eclogites have lower whole-rock high field strength element (HFSE) abundances (i.e. Zr, Hf, Nb) and Sr concentrations than Type I and II_{No} eclogites, with the Type II_L having significantly stronger Zr/Hf fractionation than all other eclogites at Roberts Victor (Fig. 8). The Type II_{No} eclogites are comprised of four eclogites with different REE$_N$ patterns from one another, but collectively differ from Type II_L and II_H eclogites primarily based on their lack of LREE-depletion (Fig. 7). The Type II_{No} eclogites have REE$_N$ and extended trace-element patterns more like some Type I eclogites, which includes relative enrichments in HFSE, LREE, and Sr compared with the Type II_L and II_H eclogites (Figs 7 and 8).

In addition, garnets from Type II_{No} eclogites have $\delta^{18}O$ values ($\delta^{18}O = 4.7$ to 6.6‰, $n = 4$) that overlap with Type I eclogitic garnet $\delta^{18}O$ values ($\delta^{18}O = 5.0$ to 9.1‰, $n = 51$) and are close to the canonical mantle range (Fig. 4a). Garnets from Type II_L and II_H eclogites have $\delta^{18}O$ values overlapping with or below the mantle range, with Type II_L eclogites having lower $\delta^{18}O$ values ($\delta^{18}O = 1.1$ to 3.6‰, $n = 20$) than Type II_H ($\delta^{18}O = 4.6$ to 4.8‰, $n = 3$). Amongst the Type II eclogites, Type II_L eclogites generally have higher calculated temperature–pressure conditions (average 1130°C and 54 kbar, $n = 28$) than the Type II_H eclogites (average 980°C and 45 kbar, $n = 5$; Fig. 5).

Type II_{No} eclogites have a wider range of calculated temperature–pressure conditions with no clear mode (range from 810 to 1240°C and 34 to 61 kbar, $n = 3$).

Roberts Victor eclogites have oceanic crust protoliths

Oxygen isotope compositions

Co-existing garnet and omphacite for eclogites in this study and published literature largely have inter-mineral $\delta^{18}O$ differences <0.65‰ (Table 3; Ongley *et al*., 1987; Beard *et al*., 1996, Radu *et al*., 2019). Therefore, we consider the $\delta^{18}O$ value of garnet as broadly representative of the bulk eclogite from which it is derived. On this basis, Type I eclogites have a $\delta^{18}O$ range that overlaps with and extends to higher values than the canonical mantle range of $\delta^{18}O = 5.5 \pm 0.4$‰ and the range for cratonic peridotite olivines (5.26 ± 0.22‰, 2σ; Regier *et al*., 2018), whereas Type II eclogites fall below the mantle range (Fig. 4a).

The range in $\delta^{18}O$ values of the full Roberts Victor eclogite suite is similar to other eclogite suites globally (Jacob, 2004; Korolev *et al*., 2018) and to rocks in some Phanerozoic ophiolites, such as the Semail ophiolite (Fig. 4; Stakes & Taylor, 1992; Ickert *et al*., 2013). The large variations in $\delta^{18}O$ values in ophiolites have been inferred to reflect previous seawater alteration of oceanic crust, which at low temperatures (< ~ 350°C) increases and at high temperatures (> ~350°C) decreases $\delta^{18}O$ values relative to the mantle range (Muehlenbachs & Clayton, 1972a, 1972b; Clayton *et al*., 1975; Gregory & Taylor, 1981). Type I eclogites have $\delta^{18}O$ values comparable to pillow lavas and sheeted dikes in the Semail ophiolite. The lower $\delta^{18}O$ values in the Type II eclogites are more comparable to some Semail ophiolite gabbros, altered at higher temperatures deeper in the oceanic crust.

In contrast to the widely-accepted model of hydrothermal alteration in the oceanic crust driving oxygen-isotope diversity in eclogites, Gréau *et al*. (2011) and Huang *et al*. (2012) proposed that the Roberts Victor Type I eclogites represent Type II eclogites that were fluid/melt-metasomatised at high temperatures in the mantle – by carbonatitic-kimberlitic spectrum melts – which shifted Type II $\delta^{18}O$ values from below the mantle range to Type I $\delta^{18}O$ values higher than the mantle range. However, the oxygen isotope composition of mantle fluids is strongly buffered by peridotitic mantle (Riches *et al*., 2016; Czas *et al*., 2018), making the persistence and effectiveness of mantle fluids with exotic oxygen-isotope compositions short-lived. A mantle metasomatic model for generating the diverse geochemical characteristics of the Roberts Victor eclogite suite also does not account for why the Type II eclogites have $\delta^{18}O$ values sometimes far below the mantle range, when values within the canonical mantle range should be expected for a mantle origin. Radu *et al*. (2019) concluded that the oxygen isotope compositions of the Roberts Victor eclogites are inherited from oceanic crust protoliths.

If the $\delta^{18}O$ values of the Roberts Victor Type II eclogites were inherited from oceanic protoliths that were altered by seawater at high temperature (> 350 to 400°C) prior to subduction, as concluded in previous studies (Jagoutz *et al*., 1984; MacGregor & Manton, 1986; Jacob, 2004; Radu *et al*., 2019), these high temperatures of alteration typically translate to great stratigraphic depths in oceanic lithosphere – i.e. within the range of gabbros in ophiolites (Fig. 4). Type I eclogites have a higher $\delta^{18}O$ range consistent with low temperature hydrothermal alteration (< 350°C), similar to the alteration regime proposed for lavas and sheeted dikes from ophiolites.

Major- and trace-element compositions

Despite the wide acceptance of an oceanic crust origin for mantle eclogites at Roberts Victor (e.g. MacGregor & Manton, 1986; Schulze *et al*., 2000; Jacob & Jagoutz, 1994; Radu *et al*., 2019), the exact nature of the lithological units from the oceanic crust that acted as protoliths for Type I and II eclogites is debated. Type I eclogites have Eu-anomalies that range from negative to positive values (Fig. 9a), that may indicate igneous protoliths that fractionated or accumulated plagioclase, respectively (MacGregor & Manton, 1986; Jacob, 2004). Type I eclogites also have positive Sr-anomalies that negatively correlate with Nd_N, and a negative correlation between ΣHREE and Eu-anomalies similar to whole-rock troctolite compositions from the Pito Deep (southeast Pacific Ocean) and other cratonic eclogite suites such as Kuruman and Kaalvallei, Kaapvaal craton (Fig. 9; Schmickler *et al*., 2004; Viljoen *et al*., 2005). Some Type I eclogites are kyanite-bearing with positive whole-rock Eu-anomalies (e.g. Radu *et al*., 2019); the occurrence of kyanite in some mantle eclogites has been ascribed to Al-rich oceanic cumulate protoliths, such as gabbros or troctolites (Shu *et al*., 2016, Radu *et al*., 2019). Conversely, some Type I eclogites have negative or only moderate positive Eu-anomalies, commonly associated with elevated LREE ($Sm_N/Nd_N < 1$; Fig. 7). These features may reflect incompatible element-rich oceanic lavas as protoliths (Beard *et al*., 1996). Bimineralic eclogites with negative or moderate-positive Eu-anomalies may also have oceanic cumulate protoliths that originally were metamorphosed to kyanite-bearing eclogites, and subsequently underwent subsolidus kyanite breakdown to form bimineralic eclogites (Sommer *et al*., 2017). Therefore, the population of Type I eclogites derived from low pressure igneous oceanic crustal protoliths that likely were compositionally heterogeneous and formed from a variety of processes.

Type II eclogites on the other hand generally have stronger positive Eu- and Sr-anomalies—particularly the Type II_L and II_H varieties—and, like Type I eclogites, show co-variations between ΣHREE and extent of Eu-anomalies, and between size of Sr-anomalies and Nd_N, similar to oceanic troctolites (Fig. 9). The Type II eclogites generally have very low incompatible element contents relative to Type I eclogites, including LREE, Sr, and HFSE (Zr, Hf; Figs 7 and 8) which can be inherited from gabbro or troctolite protoliths containing incompatible element-poor minerals, including olivine and plagioclase (Beard *et al*., 1996; Schmickler *et al*., 2004).

Beyond the presence of olivine and plagioclase in the cumulate protoliths, clinopyroxene accumulation can account for low whole-rock Zr/Hf ratios, particularly in Type II_L eclogites (clinopyroxene has $D_{Zr}/D_{Hf} \sim 0.50$; Fig. 10a; Hart & Dunn, 1993). Considering the Type II_L eclogites, we infer that those with the lowest whole-rock Zr/Hf ratios (~ 6) precipitated earliest from their parental magmas. During successive precipitation from a melt, clinopyroxene with $D_{Zr} < D_{Hf}$ will preferentially deplete the parental magma of Hf. Successively-crystallising clinopyroxene will thus have increasing Zr/Hf ratios that may correspond with decreasing Ca# (Fig. 10a). The Ca# is expected to be enhanced in Type II eclogites due to accumulation of clinopyroxene in the protoliths, which is apparent when compared to Type I eclogites with the same whole-rock Na_2O contents (Figs 10a and 10b). The Type II_L eclogites with the highest Zr/Hf ratios (~ 19) likely precipitated later. As Zr/Hf ratios increase, whole-rock Sr-anomalies, Eu-anomalies, Na_2O, and Ca# all decrease and MgO, FeO, and Mg# increase (e.g. Fig. 10).

These trends likely reflect a combination of major element fractionation trends in the magma during mineral precipitation, further documented by a positive correlation between whole-rock Mg# and Ni (Fig. 11a) and negative correlations of Mg# with Ca# (Fig. 11b) and with TiO_2 (Fig. 11c). These trends are also broadly apparent in, though off-set from, Type I eclogites, Pito Deep troctolites, and

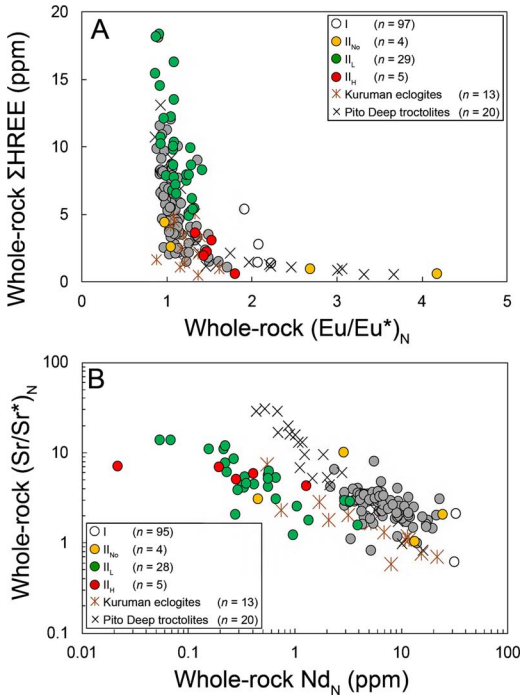

Fig. 9. (a) Reconstructed whole-rock $(Eu/Eu^*)_N$ ($Eu^* = 0.5 \times [Sm_N + Gd_N]$) and ΣHREE (Tb to Lu, ppm) normalised to C1 chondrite (McDonough & Sun, 1995) for Roberts Victor eclogites, and (b) whole-rock Nd_N and $(Sr/Sr^*)_N$, ($Sr^* = 0.5 \times [Pr_N + Nd_N]$) normalised to chondrite. Eclogite data are from this study and published literature. Data are compared with whole-rock compositions of oceanic crust troctolites from Pito Deep, southeast Pacific Ocean (Perk *et al.*, 2007), and whole-rock eclogite compositions from Kuruman, Kaapvaal craton (Schmickler *et al.*, 2004).

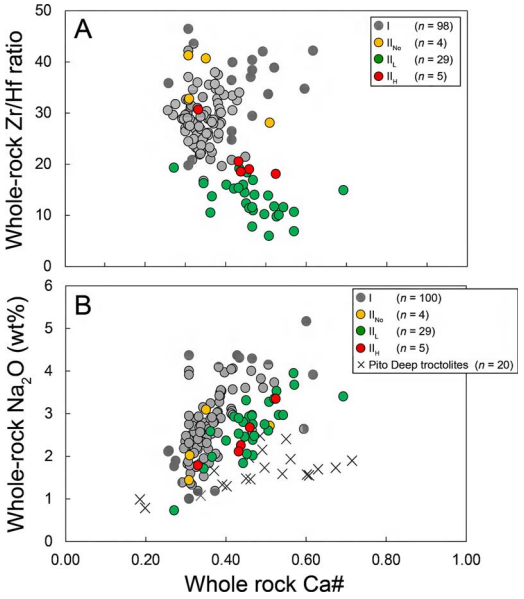

Fig. 10. Reconstructed whole-rock molar Ca# (Ca/[Ca + Mg]) for Roberts Victor eclogites from this study and published literature. Ca# is compared with whole-rock (a) Zr/Hf ratios and (b) Na_2O (oxide wt%). Data in (b) are compared with whole-rock troctolite compositions from Pito Deep, southeast Pacific Ocean (Perk *et al.*, 2007). No Zr or Hf data are reported by Perk *et al.* (2007) for Pito Deep troctolites.

eclogites from Kuruman and Kaalvallei. For the Kuruman eclogites their low HFSE and LREE contents are taken to reflect their incompatibility in plagioclase, clinopyroxene, and olivine in oceanic cumulate protoliths (Schmickler *et al.*, 2004).

Metasomatism of Roberts Victor eclogites

Type I eclogites have elevated incompatible element contents—including LREE, HFSE, and Sr— relative to Type II eclogites (Table 1). Type I eclogites are also described as having disequilibrium-type textures characterised by garnet within a 'matrix' of omphacite, whereas Type II eclogites commonly have 'equilibrium-type' textures characterised by straight, polygonal grain boundaries (Gréau *et al.*, 2011; Huang *et al.*, 2012). Previous studies have interpreted the textural differences to indicate that Type I eclogites are metasomatized and that Type II eclogites are comparatively much less altered (e.g. Gréau *et al.*, 2011; Huang *et al.*, 2012).

On this basis, Gréau *et al.* (2011) and Huang *et al.* (2012) proposed that Type I eclogite elemental and isotopic compositions were achieved through interaction between Type II eclogites and carbonatite-kimberlite spectrum magmas. Huang *et al.* (2014a) also described a Roberts Victor Type I eclogite with heterogeneous textures as well as ranges of elemental and isotopic compositions which they ascribed to progressive metasomatism by kimberlite-carbonatite-related fluids. Elazar *et al.* (2021) recently analysed fluid inclusions in garnets from a kyanite-bearing Type I eclogite and found compositional similarities to some high-density fluids in diamonds. Those authors suggested that the fluids could explain some of the compositional variation within the Type I eclogite suite.

However, Aulbach *et al.* (2020) found no clear evidence that Type I eclogite compositions are the product of metasomatism as typical indicators of mantle metasomatism are absent: Type I eclogites do not uniformly display enrichment in LREE relative to HREE, and clinopyroxenes are neither jadeite-rich nor excessively Mg-rich. Instead, Aulbach *et al.* (2020) suggested that correlations between whole-rock Eu-anomalies and ΣHREE in the Roberts Victor eclogite suite are consistent with trends of fractional crystallisation and accumulation at low pressures (i.e. Fig. 9a). The combined compositional evidence in this study, which includes major- and trace-element compositions and oxygen isotope values, suggests that the eclogite elemental compositions were largely inherited from original oceanic crust protolith compositions rather than produced or strongly modified during secondary mantle metasomatism.

Are Type II eclogites partial melt residues?

The low incompatible element contents of some cratonic eclogites may derive from partial melt extraction from their crustal protoliths or following subduction and eclogite metamorphism (Viljoen *et al.* 2005; Shu *et al.* 2018), which could account for the low incompatible element contents of the Type II eclogites. During subduction of oceanic crust, basalt and gabbro may experience partial melting and become incompatible element depleted. Residues of partial melt extraction from metabasalt will develop strong negative Sr-anomalies and experience only a slight fractionation of Zr from Hf (see modelling of Barth *et al.*, 2002, Smart *et al.*, 2017b). Partial melting of metagabbro will produce residues with decreased REE but without significant fractionation of LREE from HREE (e.g. Smart *et al.*, 2017a, 2017b). Partial melting of anhydrous eclogite (using an inferred eclogite mineralogy of 50% garnet and 50% clinopyroxene) leads to incompatible element depletion in eclogite residues (Fig. 12a;

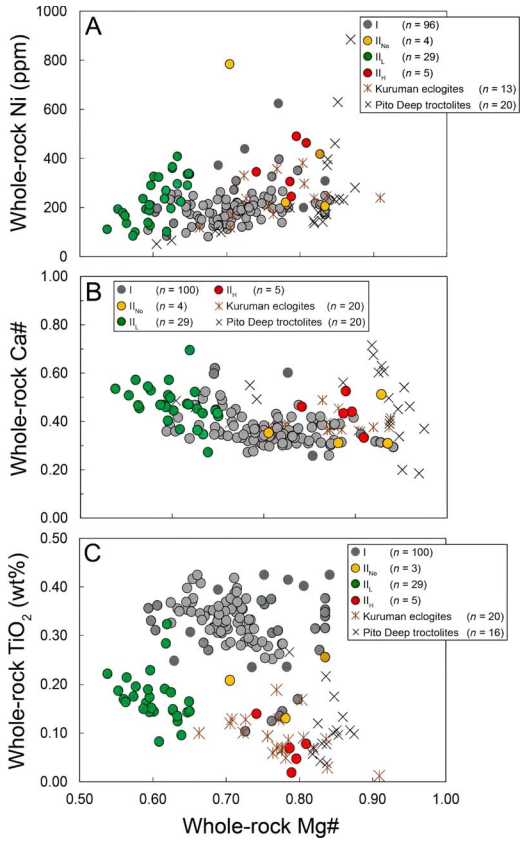

Fig. 11. (a) Reconstructed whole-rock molar Mg# (Mg/[Mg + Fe]) versus Ni (ppm), (b) Mg# versus Ca#, and (c) Mg# versus TiO_2 (oxide wt%) for Roberts Victor eclogites in this study and published literature. Data are compared with whole-rock eclogite compositions from Kuruman, Kaapvaal craton and whole-rock troctolite compositions from Pito Deep, southeast Pacific Ocean (Perk *et al.*, 2007).

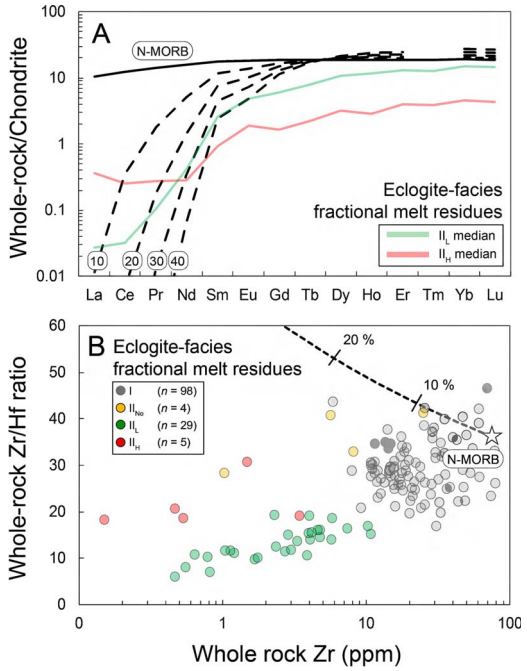

Fig. 12. Residue compositions for non-modal, anhydrous fractional melt extraction from eclogite (50% garnet, 50% clinopyroxene) with an N-MORB starting composition (Sun & McDonough, 1989). We assume equal contribution to the melt for garnet and clinopyroxene, i.e. equal melting modes. Mineral-melt partition coefficients are from Green *et al.* (2000). Modelling is after Shu *et al.* (2018). (a) Bulk REE_N patterns for eclogite melt residues (dashed lines) are compared with the median Roberts Victor Type II_L and II_H compositions. Percentage of melting is indicated by a number. (b) The Zr abundance and Zr/Hf ratios of modelled residues, with the percentage of melting indicated by a number. Residues are compared with whole-rock Roberts Victor eclogite compositions from this study and published literature.

Smart *et al.* 2017b; Shu *et al.*, 2018), but increasing Zr/Hf ratios that evolve away from the Type II_L eclogite compositions (Fig. 12b). Therefore, the combination of $LREE_N$-depleted compositions and the extremely varied, low Zr/Hf ratios of the Type II_L eclogites in particular cannot be explained solely by partial melting.

Rutile can also affect bulk-rock reconstructions as it is a Ti-rich mineral with high mineral-melt partition coefficients for the HFSE Zr and Hf. All Roberts Victor eclogites have negative whole-rock Ti-anomalies when reconstructed using garnet and omphacite only, which may correspond to 'missing' rutile, though some eclogites may also inherit negative Ti-anomalies from cumulate protoliths (Aulbach, 2020). One possible explanation for missing rutile in the eclogite assemblage at Roberts Victor is rutile loss during partial melting. However, rutile has a marginally lower Zr/Hf ratio than coexisting melt (Foley *et al.*, 2000) and consequently, rutile extraction should not be associated with significantly decreasing Zr/Hf ratios in the residues.

In addition, Type II eclogite garnet and omphacite in this study contain a low abundance (< 1 vol%) of small rutile needles. The compositions of rutile needles in Type II eclogite minerals have been previously reported by Jacob *et al.* (2005). For example, Type II eclogite BD 1191 reported by Jacob *et al.* (2005) has low whole-rock Zr (2.76 ppm), Hf (0.245 ppm), and Zr/Hf ratio (11.3) calculated using garnet and omphacite only. Rutile needles from sample BD 1191 have Zr (285 ppm) and Hf (17.8 ppm) concentrations and subchondritic Zr/Hf ratios (16.0) that, even when added in large quantities (1%) into the whole-rock reconstructions, cannot increase whole-rock Zr, Hf, or Zr/Hf ratios to Type I eclogite levels. Jacob *et al.* (2005) inferred the needles to have exsolved from the host minerals, inheriting low HFSE concentrations and Zr/Hf ratios from them. For the new eclogites in our study, Zr and Hf concentrations in garnet and omphacite were determined by LA-ICP-MS with a 130 μm spot size, which likely included some rutile needles in the ablated volume. Measured garnet and omphacite trace-element compositions thus likely already account, at least in part, for the presence of minor rutile.

Instead, low Zr/Hf ratios of the Type II eclogites could be inherited from an oceanic protolith as has been inferred for some other cratonic eclogites globally (Aulbach *et al.*, 2011), rather than require a partial melting origin. On this basis, we conclude that the elemental compositions of the Type II eclogites—including their low incompatible element contents and low Zr/Hf ratios—are largely a protolith feature and not dominated by partial melt loss with or without rutile.

Parental magma compositions of Roberts Victor eclogite protoliths

Comparison with ophiolites

Oceanic crust is generated from magmas extracted from depleted MORB mantle (DMM) by near-fractional melting: early incipient

melts of upward-convecting DMM will be chemically more enriched than late-stage melts (e.g. Johnson *et al.*, 1990; Pearce & Parkinson 1993; Nonnotte *et al.*, 2005). These melts are commonly mixed and aggregated into the MORB composition. Based on whole-rock MgO > 12 wt% (Aulbach & Jacob, 2016) many Roberts Victor eclogites classify as 'picritic' rather than basaltic, possibly related to higher mantle temperatures (Labrosse & Jaupart, 2007; Herzberg *et al.*, 2010) at the time of Archean protolith formation (older than to the reported eclogite age of ~2.7 ± 0.1 Ga; Jagoutz *et al.*, 1984; Jacob *et al.*, 2005). However, the mean ± 2σ range of Archean picrite REE compositions and Zr/Hf ratios (GEOROC database; http://georoc.mpch-mainz.gwdg.de) overlaps with that of N-MORB (Sun and McDonough 1989), and Stachel *et al.* (2004) demonstrated that the average parental melt of eclogitic diamond inclusions has a MORB-like REE composition.

In natural systems oceanic crust may be compositionally heterogeneous. For example, Piccardo & Guarnieri (2011) described gabbronorite cumulates and gabbroic dikes within oceanic peridotites from the Alpine-Apennine ophiolite (Corsica). The gabbronorites contain clinopyroxene with subchondritic LREE abundances, low Zr abundances, low Zr/Hf ratios, and stronger LREE-depletion than clinopyroxene in equilibrium with MORB (inset image in Fig. 13a). Those authors concluded that the gabbronorite cumulates precipitated from unaggregated (unmixed) fractional melts of mantle sources that had previously undergone 5%–7% spinel-facies fractional melt extraction. Conversely, gabbroic dikes cross-cut the gabbronorites and contain clinopyroxene with an order of magnitude higher LREE as well as higher Zr abundances and Zr/Hf ratios (Fig. 13a). Piccardo & Guarnieri (2011) concluded that the gabbroic dikes formed from aggregated MORB magmas instead.

We compare the trace-element composition of clinopyroxene from rocks described by Piccardo & Guarnieri (2011) with whole-rock compositions of eclogites from Roberts Victor on the basis of high D_{Zr}, D_{Hf}, and D_{REE} (crystal-melt) in clinopyroxene versus other low-pressure cumulate phases such as plagioclase or olivine (Hart & Dunn, 1993; Bédard, 1994; Blundy *et al.*, 1998). Therefore, clinopyroxene controls the budget of these trace-elements in the bulk cumulate, including the Zr/Hf ratio. The HFSE compositions of Roberts Victor Type I eclogites occur within the range of global ophiolite-hosted lavas and cumulates (Fig. 13b) and have higher Zr concentrations and Zr/Hf ratios than clinopyroxene in equilibrium with MORB. The Type I eclogites have similar HFSE compositions to clinopyroxene from Alpine-Apennine gabbroic dikes that formed from MORB. Conversely, Type II eclogites, particularly the Type II_L eclogites with Zr/Hf ratios down to ~6, have a compositional range that overlaps ophiolite cumulates but not lavas, lower than the composition of clinopyroxene in equilibrium with MORB. These eclogites have similar HFSE compositions to the clinopyroxene from Alpine-Apennine gabbronorites that formed from melts of mantle that experienced previous melt extraction.

Type II_L eclogites are unlikely to have inherited their low Zr/Hf ratios from protoliths formed from N-MORB, as they have lower Zr/Hf ratios than clinopyroxene in equilibrium with N-MORB (Fig. 13a). However, these ratios can reflect oceanic protoliths that formed from melts with compositions distinct from MORB: Aulbach *et al.* (2011) suggested that low Zr/Hf ratios in some cratonic eclogites were inherited from protoliths relating to melts of mantle sources that had already experienced previous melting in equilibrium with clinopyroxene, to fractionate Zr/Hf. Type I eclogites have a range of whole-rock Zr abundances and Zr/Hf ratios higher than clinopyroxene in equilibrium with N-MORB (Fig. 13a).

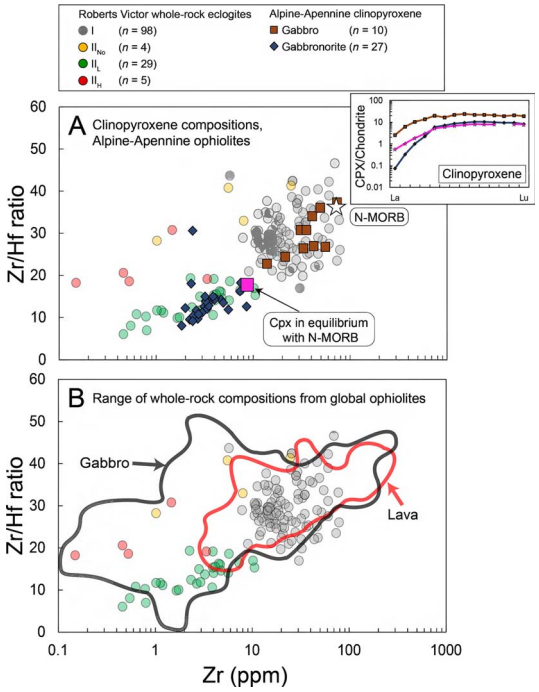

Fig. 13. (a) Roberts Victor whole-rock eclogite compositions compared with the compositions of clinopyroxenes from gabbros and gabbronorites from Alpine-Apennine ophiolites (Piccardo & Guarnieri, 2011). Shown also are the compositions of N-MORB (Sun & McDonough, 1989) and the clinopyroxene in equilibrium with N-MORB, calculated using the mineral-melt partition coefficients of Hart & Dunn (1993). The inset image compares the median REE_N patterns of clinopyroxenes from gabbronorites (dark blue) and gabbros (brown) from Alpine-Apennine ophiolites (Piccardo & Guarnieri, 2011) with the REE_N pattern of clinopyroxene calculated to be in equilibrium with N-MORB (pink). (b) Distribution of Roberts Victor whole-rock eclogite compositions from this study and the literature, compared with fields of whole-rock compositions from Cretaceous ophiolites globally (n = 774). Ophiolite data were obtained from the PetDB Database (www.earthchem.org/petdb) on 24 April 2021, using the parameter tectonic setting: ophiolite. The 'lava' field contains rocks classified as 'basalt' and 'tholeiite' by PetDB.

Consequently, the protoliths of Type I eclogites could have been oceanic lavas and cumulates formed from N-MORB-like magmas (Radu *et al.*, 2019).

Modelling the Type II_L protolith parental melt composition

Based on the similar range in Zr abundance and Zr/Hf ratios of Roberts Victor Type II eclogites and clinopyroxene from gabbronorites of the Alpine-Apennine ophiolites, we speculate that many Type II eclogites have protoliths that formed as cumulates from magmas compositionally similar to unaggregated melts extracted from DMM. In contrast, Type I eclogite protoliths may have formed from aggregated MORB-like magmas, i.e. their protoliths were melts, or cumulates, formed from melts with MORB-like compositions.

To evaluate the scenario that Type II eclogites have oceanic protoliths that formed from magmas other than MORB *sensu stricto*, we calculate the trace-element composition of fractional melts from DMM. We follow previous workers and model anhydrous fractional melt extraction from model spinel- and garnet-lherzolite (e.g. Johnson *et al.*, 1990; Hellebrand *et al.*, 2002; Weyer *et al.*, 2003; Warren, 2016), using REE and HFSE as process monitors. The employed fractional melting equations of Johnson *et al.* (1990), starting trace-element composition (DMM; Workman & Hart, 2005), starting

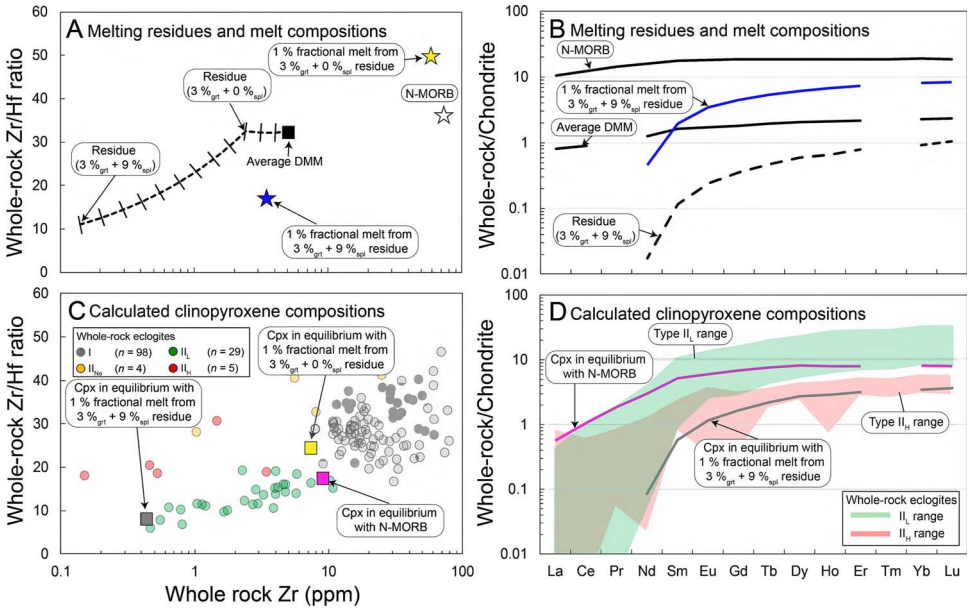

Fig. 14. Modelling results for non-modal fractional melting of a rock with a starting trace-element composition of DMM (Workman & Hart, 2005). See section *Modelling the Type II$_L$ protolith parental melt composition* and Supplementary Online Data Appendix 5 for modelling conditions. The rock undergoes 3% melting as garnet-lherzolite followed by a further 9% as spinel-lherzolite. (a) Zr abundance and Zr/Hf ratio of the modelled residues (dashed line) with tick marks indicating 1% melting increments. The degree of melting is indicated next to two residues based on combined garnet-facies melting (subscript $_{grt}$) and spinel-facies melting (subscript $_{spl}$). The compositions of two 1% fractional melts extracted from spinel-lherzolite residues are shown following (i) 3% garnet-facies melting, and (ii) a combined 3% garnet-facies and 9% spinel-facies melting. The compositions of N-MORB (Sun & McDonough, 1989) and average DMM are shown. (b) The REE$_N$ pattern (normalised to chondrite; McDonough & Sun, 1995) of a DMM residue following a combined 3% garnet-facies and 9% spinel-facies melting is shown (dashed line), as well as the composition of the 1% fractional melt extracted from this residue (blue line). The compositions of N-MORB and average DMM are shown. (c) The HFSE composition of clinopyroxene in equilibrium with N-MORB is compared to the composition of clinopyroxene calculated to be in equilibrium with two 1% fractional melts extracted from DMM residues (spinel-lherzolite) following (i) 3%$_{grt}$ + 0%$_{spl}$ melting, and (ii) 3%$_{grt}$ + 9%$_{spl}$ melting. Clinopyroxene compositions are calculated using the mineral-melt partition coefficients of Hart & Dunn (1993). (d) The REE$_N$ pattern of clinopyroxene in equilibrium with N-MORB is compared with the composition of clinopyroxene calculated in equilibrium with the 1% fractional melt extracted from DMM (spinel-lherzolite) following 3%$_{grt}$ + 9%$_{spl}$ melting. These compositions are compared with the range of whole-rock REE$_N$ patterns for Type II$_L$ and II$_H$ eclogites.

mineralogy, and melting proportions for model garnet-lherzolite and spinel-lherzolite are described in Supplementary Online Data Appendix 5. We model polybaric melting with minor amounts of garnet-facies melting (3%) followed by larger amounts of spinel-facies melting (9%; for further discussion see Johnson *et al*., 1990, Hellebrand *et al*., 2002, Warren, 2016).

Unsurprisingly (c.f., Aulbach *et al*., 2011), the calculated melt compositions extracted from depleted residues are chemically less-enriched than those from comparatively fertile starting compositions, with lower LREE and Zr abundances and Zr/Hf ratios (Figs 14a and 14b). This is apparent in the HFSE and REE composition of 1% fractional melts extracted at spinel-facies from DMM following (1) a total 3% fractional melting at garnet-facies, and (2) a total combined 3% fractional melting at garnet-facies followed by 9% at spinel-facies (12% total melting; Figs 14a and 14b).

The clinopyroxene in equilibrium with the melt extracted from a DMM residue after 3% garnet-facies melting has a similar Zr abundance and Zr/Hf ratio to the clinopyroxene calculated in equilibrium with N-MORB (Fig. 14c). Conversely, the clinopyroxene calculated in equilibrium with the melt extracted from the DMM residue after 12% total melting has lower whole-rock Zr/Hf ratios and Zr abundances, similar to the Type II$_L$ eclogites (Figs 14b and 14c), also mimicking their fractionated LREE/MREE nature (although at lower concentrations; Fig. 14d).

We conclude that many Roberts Victor Type II$_L$ eclogites had oceanic cumulate protoliths formed from magmas extracted from depleted mantle sources that had experienced prior extraction of MORB-like melts. In such a model the Type I eclogites, with higher Zr/Hf ratios and incompatible element contents, may have formed as crystallised melts or as cumulates from this earlier melting event, or may be completely unrelated. This conclusion is in keeping with results from other localities. Jacob & Foley (1999) suggested that some Siberian eclogites with ultra-depleted HFSE compositions had oceanic crust protoliths, such as basalts or intrusive rocks, whose parental magma derived from a previously depleted mantle source. Aulbach *et al*. (2011) described 'boninite-like' eclogites from the Slave craton with subchondritic Zr/Hf ratios that relate to early clinopyroxene-controlled melting of the mantle source during protolith generation. Viljoen *et al*. (2005) reported 'Group I' and 'Group II' eclogites from Kaalvallei with significant differences in major- and trace-element composition, similar to differences between Roberts Victor Type I and II eclogites. Those authors inferred that the protoliths of the two suites of eclogites could have formed from different parental melts. For Roberts Victor, if the protoliths of Type II eclogites formed in an oceanic ridge environment, their parental melt must have escaped mixing with earlier-formed, more enriched melts, possibly by lateral injection into oceanic crust (e.g. Piccardo & Guarnieri, 2011; Basch *et al*., 2019).

Sources of Type II_H and II_{No} eclogites

Roberts Victor Type II_H eclogites have $\delta^{18}O$ values ($\delta^{18}O = 4.6$ to 4.8‰) slightly below the mantle range but within the range for gabbros from ophiolites (Fig. 4). The Type II_H eclogites have positive whole-rock Eu- and Sr-anomalies indicating that they had plagioclase-bearing cumulate protoliths (Fig. 9). Their whole-rock REE_N patterns are similar to Type II_L eclogites but they have higher Mg# and lower incompatible element contents ($\sum$REE, TiO_2, Sr; Figs 7, 8 and 11). Both Type II_H and II_L eclogites have significantly lower abundances of incompatible elements than Type I eclogites (i.e. Zr, Hf, Sr, LREE; Figs 7 and 8) consistent with the proposed cumulate origin of the Type II eclogites. A possible explanation for the higher Zr/Hf ratios of Type II_H relative to Type II_L eclogites is that Type II_H protoliths formed from a more MORB-like magma with different Zr/Hf systematics. Alternatively, Type II_H protoliths could have formed from a magma with a similar elemental composition to Type II_L protoliths but with radically different proportions of liquidus minerals crystallising/accumulating, possibly due to a change in pressure or water content (Presnall *et al.*, 1978; Feig *et al.*, 2006). The higher positive Eu-anomalies and Mg# of Type II_H eclogites (Figs 9a and 11) could reflect crystallisation/accumulation of higher abundances of olivine and plagioclase relative to clinopyroxene. Type II_H eclogites could have precipitated early as clinopyroxene-poor olivine- and plagioclase-rich cumulates and Type II_L eclogites could have formed subsequently from the same magma following earlier olivine fractionation, as comparatively clinopyroxene-rich cumulates, accounting for their lower bulk rock Ni and Mg# (Fig. 11).

The Type II_{No} eclogites have Type II textures but lack the significant incompatible element depletion that characterises the Type II_L and II_H eclogites. Their extended trace-element patterns and Zr/Hf ratios are similar to Type I eclogites (Figs 7, 8, and 10), suggesting that their protoliths crystallised from parental magmas with more N-MORB-like trace-element compositions. Type II_{No} eclogite $\delta^{18}O$ values overlap those of Type I eclogites and the canonical mantle range (Fig. 4a) suggesting that their protoliths resided at shallower stratigraphic depth in the oceanic crust than other Type II protoliths, possibly as sheeted dikes.

SUMMARY

A new study of 63 eclogites from the former Roberts Victor Mine has strengthened the applicability of the textural and chemical classification of these eclogites into two main classes. We propose a new model to explain the incompatible element-poor compositions of Type II eclogites relative to Type I eclogites. Type II eclogites typically have $\delta^{18}O$ values far below the canonical mantle value, accompanied by positive Sr- and Eu-anomalies, indicating that their protoliths crystallised as plagioclase-bearing cumulates at deep levels of oceanic crust ($\geq$ 2 km). Type II eclogites also show extreme fractionation of Zr from Hf in their reconstructed bulk compositions. The newly defined Type II_L and II_H eclogites have low incompatible trace-element contents compared with Type I eclogites, as well as positive $MREE_N$-$HREE_N$ slopes. Modelling demonstrates that the $LREE_N$-depletion and low Zr/Hf ratios ($< \sim 19$) of Type II eclogites cannot be achieved purely due to secondary melt extraction, during or after subduction. Instead, we show that the incompatible element depletion and low Zr/Hf ratios in Type II eclogites are consistent with protolith crystallisation from melts chemically less-enriched than N-MORB. Successive decompression melting of a clinopyroxene-bearing depleted mantle source during upwelling at a mid-ocean ridge produces residues with increasing depletion in incompatible elements and decreasing Zr/Hf ratios, similar to the systematics observed in Type II_L eclogites. Late-stage melts of such depleted residues are less incompatible element enriched than an aggregated N-MORB melt. Such late-stage melts may precipitate clinopyroxene-bearing cumulates depleted in incompatible elements and with low Zr/Hf ratios. As recent analogues, cumulate gabbros in Phanerozoic ophiolites extend towards the composition of Type II_L eclogites (Fig. 13).

ACKNOWLEDGEMENTS

This study represents a portion of M.F.H.'s PhD research. Yuri Kinakin and Diavik Diamond Mines (2012) Inc. are thanked for financial support of this project. We thank Valentin Troll for his editorial treatment of this manuscript, as well as Dorrit Jacob and two anonymous reviewers for their comments which improved its quality. The authors thank Tom Chacko, Bob Luth, Herman Grütter, Fanus Viljoen, Gerhard Brey, Karen Smit, and Karlis Muehlenbachs for useful discussions and comments. The analytical assistance of Andrew Locock, Yan Luo, and Robert Dokken is greatly appreciated.

DATA AVAILABILITY

The data supporting this article are available in the article and in its online supplementary material.

FUNDING

This work was supported by a Natural Sciences and Engineering Research Council of Canada Collaborative Research and Development Grant in partnership with Diavik Diamond Mines (2012) Inc. (DRCPJ 476392 to T.S. and D.G.P.), a Natural Sciences and Engineering Research Council of Canada Discovery Grant to T.S., a Canada Excellence Research Chair award to D.G.P., and a National Science Foundation grant to Z.D.S. (NSF EAR 1903852).

REFERENCES

Aulbach, S. (2020). Temperature-dependent rutile solubility in garnet and clinopyroxene from mantle eclogite: implications for continental crust formation and V-based oxybarometry. *Journal of Petrology*, **61**, 1–26.

Aulbach, S. & Jacob, D. E. (2016). Major- and trace-elements in cratonic mantle eclogites and pyroxenites reveal heterogeneous sources and metamorphic processing of low-pressure protoliths. *Lithos*, **262**, 586–605.

Aulbach, S., Massuyeau, M., Garber, J., Gerdes, A., Heaman, L. M. & Viljoen, K. S. (2020). Ultramafic carbonated melt- and auto-metasomatism in mantle eclogites: Compositional effects and geophysical consequences. *Geochemistry, Geophysics, Geosystems*, **21**, 1–27.

Aulbach, S. A., O'Reilly, S. Y. & Pearson, N. J. (2011). Constraints from eclogite and MARID xenoliths on origins of mantle Zr/Hf-Nb/ta variability. *Contributions to Mineralogy and Petrology*, **162**, 1047–1062.

Baertschi, P. (1976). Absolute ^{18}O content of standard mean ocean water. *Earth and Planetary Science Letters*, **31**, 341–344.

Barth, M. G., Foley, S. F. & Horn, I. (2002). Partial melting in Archean subduction zones: Constraints from experimentally determined trace element partition coefficients between eclogitic minerals and tonalitic melts under upper mantle conditions. *Precambrian Research*, **113**, 323–340.

Basch, V., Rampone, E., Borghini, G., Ferrando, C. & Zanetti, A. (2019). Origin of pyroxenites in the oceanic mantle and their implications on the reactive percolation of depleted melts. *Contributions to Mineralogy and Petrology*, **174**, 97.

Beard, B. L., Fraracci, K. N., Taylor, L. A., Snyder, G. A., Clayton, R. A., Mayeda, T. K. & Sobolev, N. V. (1996). Petrography and geochemistry of eclogites from the Mir kimberlite, Yakutia, Russia. *Contributions to Mineralogy and Petrology*, **125**, 293–310.

Bédard, J. H. (1994). A procedure for calculating the equilibrium distribution of trace elements among the minerals of cumulate rocks, and the concentration of trace elements in the coexisting liquids. *Chemical Geology*, **118**, 143–153.

Blundy, J. D., Robinson, J. A. C. & Wood, B. J. (1998). Heavy REE are compatible in clinopyroxene on the spinel lherzolite solidus. *Earth and Planetary Science Letters*, **160**, 493–504.

Cano, E. J., Sharp, Z. D. & Shearer, C. K. (2020). Distinct oxygen isotope compositions of the earth and moon. *Nature*, **13**, 270–274.

Caporuscio, F. A. (1990). Oxygen isotope systematics of eclogite mineral phases from South Africa. *Lithos*, **25**, 203–210.

Caporuscio, F. A. & Smyth, J. R. (1990). Trace element crystal chemistry of mantle eclogites. *Contributions to Mineralogy and Petrology*, **105**, 550–561.

Clark, J. R. & Papike, J. J. (1968). Crystal-chemical characterization of omphacites. *American Mineralogist*, **53**, 840–868.

Clayton, R. N., Goldsmith, J. R., Karel, K. J., Mayeda, T. K. & Newton, R. C. (1975). Limits on the effect of pressure on isotopic fractionation. *Geochimica et Cosmochimica Acta*, **39**, 1197–1201.

Czas, J., Stachel, T., Pearson, D. G., Stern, R. A. & Read, G. H. (2018). Diamond brecciation and annealing accompanying major metasomatism in eclogite xenoliths from the Sask craton, Canada. *Mineralogy and Petrology*(Suppl 1), **112**, S311–S323.

Dawson, J. B. & Stephens, W. E. (1975). Statistical classification of garnets from kimberlite and associated xenoliths. *Journal of Geology*, **83**, 589–607.

Dawson, J. B. (1984). Contrasting types of upper-mantle metasomatism? *Developments in Petrology*, **11**, 259–294.

Desmons, J. & Smulikowski, W. (2007) High P/T Metamorphic Rocks. In: (Fettes D. & Desmons J. (eds)) *Metamorphic Rocks: A Classification and Glossary of Terms*. Cambridge: Cambridge University Press, pp. 32–35.

Elazar, O., Kessel, R., Huang, J-X, Marquardt, K. & Navon, O. (2021). Silicic microinclusions in a metasomatized eclogite from Roberts Victor mine, South Africa. *Lithos*, **388–389**, 106057–106069.

Feig, S. T., Koepke, J. & Snow, J. E. (2006). Effect of water on tholeiitic basalt phase equilibria: an experimental study under oxidizing conditions. *Contributions to Mineralogy and Petrology*, **152**, 611–638.

Foley, S. F., Barth, M. G. & Jenner, G. A. (2000). Rutile/melt partition coefficients for trace elements and an assessment of the influence of rutile on the trace element characteristics of subduction zone magmas. *Geochimica et Cosmochimica Acta*, **64**, 933–938.

Garlick, G. D., MacGregor, I. D. & Vogel, D. E. (1971). Oxygen isotope ratios in eclogites from kimberlites. *Science*, **172**, 1025–1035.

Gréau, Y., Huang, J.-X., Griffin, W. L., Renac, C., Alard, O. & O'Reilly, S. Y. (2011). Type I eclogites from Roberts victor kimberlites: products of extensive mantle metasomatism. *Geochimica et Cosmochimica Acta*, **75**, 6927–6954.

Green, D. H. & Ringwood, A. E. (1967). An experimental investigation of the gabbro to eclogite transformation and its petrological applications. *Geochimica et Cosmochimica Acta*, **31**, 767–833.

Green, D. H. & Ringwood, A. E. (1972). A comparison of recent experimental data on the gabbro-garnet granulite-eclogite transition. *Journal of Geology*, **80**, 277–288.

Green, T. H., Blundy, J. D., Adam, J. & Yaxley, G. M. (2000). SIMS determination of trace element partition coefficients between garnet, clinopyroxene and hydrous basalt liquids at 2-7.5 GPa and 1080-1200°C. *Lithos*, **53**, 165–187.

Gregory, R. T. & Taylor, H. P. (1981). An oxygen isotope profile in a section of cretaceous oceanic crust, Samail ophiolite: Evidence for $\delta^{18}O$ buffering of the oceans by deep (>5 km) seawater-hydrothermal circulation at mid-ocean ridges. *Journal of Geophysical Research*, **86**, 2737–2755.

Grütter, H. S. (2009). Pyroxene xenocryst geotherms: techniques and application. *Lithos*, **112S**, 1167–1178.

Hardman, M. F., Pearson, D. G., Stachel, T. & Sweeney, R. J. (2018). Statistical approaches to the discrimination of crust- and mantle-derived low-Cr garnet – Major-element-based methods and their application in diamond exploration. *Journal of Geochemical Exploration*, **186**, 24–35.

Hart, S. R. & Dunn, T. (1993). Experimental cpx/melt partitioning of 24 trace elements. *Contributions to Mineralogy and Petrology*, **113**, 1–8.

Harte, B. & Kirkley, M. B. (1997). Partitioning of trace elements between clinopyroxene and garnet: data from mantle eclogites. *Chemical Geology*, **136**, 1–24.

Hasterok, D. & Chapman, D. S. (2011). Heat production and geotherms for the continental lithosphere. *Earth and Planetary Science Letters*, **307**, 59–70.

Hatton, C. J. (1978). The geochemistry and origin of xenoliths from the Roberts Victor mine. PhD thesis. University of Cape Town, Cape Town.

Hellebrand, E., Snow, J. E., Hoppe, P. & Hofmann, A. W. (2002). Garnet-field melting and late-stage refertilization in 'residual' abyssal peridotites from the central Indian ridge. *Journal of Petrology*, **43**, 2305–2338.

Helmstaedt, H. & Doig, R. (1975). Eclogite nodules from kimberlite pipes of the Colorado plateau – Samples of subducted Franciscan-type oceanic lithosphere. *Physics and Chemistry of the Earth*, **9**, 95–111.

Helmstaedt, H. & Schulze, D. J. (1989). Southern African kimberlites and their mantle sample: implications for Archaean tectonics and lithosphere evolution. In: Ross, J. (ed) *Kimberlites and Related Rocks, Vol. 1. Geological Society of Australia, Perth, Special Publication*, **14**, 358–368.

Herzberg, C., Condie, K. & Korenaga, J. (2010). Thermal history of the earth and its petrological expression. *Earth and Planetary Science Letters*, **292**, 79–88.

Huang, J.-X., Gréau, Y., Griffin, W. L., O'Reilly, S. Y. & Pearson, N. J. (2012). Multi-stage origin of Roberts Victor eclogites: progressive metasomatism and its isotopic effects. *Lithos*, **142-143**, 161–181.

Huang, J.-X., Griffin, W. L., Gréau, Y., Pearson, N. J., O'Reilly, S. Y., Cliff, J. & Martin, L. (2014a). Unmasking xenolithic eclogites: progressive metasomatism of a key Roberts Victor sample. *Chemical Geology*, **364**, 56–65.

Huang, J.-X., Li, P., Griffin, W. L., Xia, Q.-K., Gréau, Y., Pearson, N. J. & O'Reilly, S. Y. (2014b). Water contents of Roberts Victor eclogites: primary and metasomatic controls. *Contributions to Mineralogy and Petrology*, **168**, 1092.

Huang, J.-X., Xiang, Y. X., An, Y., Griffin, W. L., Gréau, Y., Xie, L., Pearson, N. J., Yu, H. & O'Reilly, S. Y. (2016). Magnesium and oxygen isotopes in Roberts Victor eclogites. *Chemical Geology*, **438**, 73–83.

Ickert, R. B. & Stern, R. A. (2013). Matrix corrections and error analysis in high-precision SIMS $^{18}O/^{16}O$ measurements of ca-mg-Fe garnet. *Geostandards and Geoanalytical Research*, **37**, 429–448.

Ickert, R. B., Stachel, T., Stern, R. A. & Harris, J. W. (2013). Diamond from recycled crustal carbon documented by coupled $\delta^{18}O$-$\delta^{13}C$ measurements of diamonds and their inclusions. *Earth and Planetary Science Letters*, **364**, 85–97.

Ireland, T. R., Rudnick, R. L. & Spetsius, Z. (1994). Trace elements in diamond inclusions from eclogites reveal link to Archean granites. *Earth and Planetary Science Letters*, **128**, 199–213.

Jacob, D. E. (2004). Nature and origin of eclogite xenoliths from kimberlites. *Lithos*, **77**, 295–316.

Jacob, D. & Jagoutz, E. (1994) A diamond-graphite bearing eclogite from Roberts Victor (South Africa): indications for petrogenesis from Pb, Nd and Sr isotopes. In: (Meyer H. O. A. & Leonardos O. H. (eds)) *Proceedings of the 5th International Kimberlite Conference, Vol. 1. Companhia de Pesquisa de Recursos Minerais*. Special Publication 1/A, pp. 304–317.

Jacob, D. E., Bizimis, M. & Salters, V. J. M. (2005). Lu-Hf and geochemical systematics of recycled ancient oceanic crust: evidence from Roberts Victor eclogites. *Contributions to Mineralogy and Petrology*, **148**, 707–720.

Jacob, D. E. & Foley, S. F. (1999). Evidence for Archean Ocean crust with low high field strength element signatures from diamondiferous eclogite xenoliths. *Lithos*, **48**, 317–336.

Jacob, D. E., Schmickler, B. & Schulze, D. J. (2003). Trace element geochemistry of coesite-bearing eclogites from the Roberts Victor kimberlite, Kaapvaal craton. *Lithos*, **71**, 337–351.

Jagoutz, E., Dawson, J. B., Hoernes, S., Spettel, B. & Waenke, H. (1984). Anorthositic oceanic crust in the Archean earth. Abstract, proceedings of the 15th Lunar and Planetary Science Conference. *Journal of Geophysical Research Supplement*, 395–396.

Johnson, K. T. M., Dick, H. J. B. & Shimizu, N. (1990). Melting in the oceanic upper mantle: an ion microprobe study of diopsides in abyssal peridotites. *Journal of Geophysical Research*, **95**, 2661–2678.

Kiseeva, E. S., Kamenetsky, V. S., Yaxley, G. M. & Shee, S. R. (2017). Mantle melting versus mantle metasomatism – "the chicken or the egg" dilemma. *Chemical Geology*, **455**, 120–130.

Korolev, N. M., Melnik, A. E., Li, X.-H. & Skublov, S. G. (2018). The oxygen isotope composition of mantle eclogites as a proxy of their origin and evolution: a review. *Earth-Science Reviews*, **185**, 288–300.

Krogh, E. J. (1988). The garnet-clinopyroxene Fe-mg geothermometer – a reinterpretation of existing experimental data. *Contributions to Mineralogy and Petrology*, **99**, 44–48.

Labrosse, S. & Jaupart, C. (2007). Thermal evolution of the earth: Secular changes and fluctuations of plate characteristics. *Earth and Planetary Science Letters*, **260**, 465–481.

MacGregor, I. D. & Carter, J. L. (1970). The chemistry of clinopyroxenes and garnets of eclogite and peridotite xenoliths from the Roberts victor mine, South Africa. *Physics of the Earth and Planetary Interiors*, **3**, 391–397.

MacGregor, I. D. & Manton, W. I. (1986). Roberts Victor eclogites: ancient oceanic crust. *Journal of Geophysical Research*, **91**, 14063–14079.

Mattey, D., Lowry, D. & Macpherson, C. (1994). Oxygen isotope composition of mantle peridotite. *Earth and Planetary Science Letters*, **128**, 231–241.

McCandless, T. E. & Gurney, J. J. (1989) Sodium in garnet and potassium in clinopyroxene: criteria for classifying eclogites. In: (Ross J., Jaques A. L., Ferguson J., Green D. H., O'Reilly S. Y., Danchin R. V. & Janse A. J. A. (eds)) *Kimberlites and Related Rocks, Geological Society of Australia Special Publication*, Vol. **2**. Oxford: Blackwell, pp. 827–832.

McDade, P. (1999). An experimental and geochemical study of the products of extreme metamorphic processes: ultrahigh-temperature granulites and the Roberts Victor eclogites. PhD thesis. University of Edinburgh, 390 pp.

McDonough, W. F. (1991). Partial melting of subducted oceanic crust and isolation of its residual eclogitic lithology. *Philosophical Transactions of the Royal Society A*, **335**, 407–418.

McDonough, W. F. & Sun, S.-s. (1995). The composition of the earth. *Chemical Geology*, **120**, 223–253.

Morimoto, N., Fabries, J., Ferguson, A. K., Ginzburg, I. V., Ross, M., Seifert, F. A., Zussman, J., Aoki, K. & Gottardi, G. (1988). Nomenclature of pyroxenes. *American Mineralogist*, **73**, 1123–1133.

Muehlenbachs, K. & Clayton, R. N. (1972a). Oxygen isotope studies of fresh and weathered submarine basalts. *Canadian Journal of Earth Sciences*, **9**, 172–184.

Muehlenbachs, K. & Clayton, R. N. (1972b). Oxygen isotope geochemistry of submarine greenstones. *Canadian Journal of Earth Sciences*, **9**, 471–478.

Nonnotte, P., Ceuleneer, G. & Benoit, M. (2005). Genesis of andesitic-boninitic magmas at mid-ocean ridges by melting of hydrated peridotites: Geochemical evidence from DSDP site 334 gabbronorites. *Earth and Planetary Science Letters*, **236**, 632–653.

O'Hara, M. J. & Yoder, H. S. (1967). Formation and fractionation of basic magmas at high pressures. *Scottish Journal of Geology*, **3**, 67–117.

Ongley, J. S., Basu, A. R. & Kyser, T. K. (1987). Oxygen isotopes in coexisting garnets, clinopyroxenes and phlogopites of Roberts Victor eclogites: implications for petrogenesis and mantle metasomatism. *Earth and Planetary Science Letters*, **83**, 80–84.

Pearce, J. A. & Parkinson, I. J. (1993) Trace element models for mantle melting: application to volcanic arc petrogenesis. In: (Prichard H. M., Alabaster T., Harris N. B. W. & Neary C. R. (eds)) *Magmatic Processes and Plate Tectonics. Geological Society Special Publication*, Vol. **76**, pp. 373–403.

Pearson, D. G. & Nixon, P. H. (1996). Diamonds in young orogenic belts: graphitized diamonds from Beni Bousera, N. Morocco, a comparison with kimberlite-derived diamond occurrences and implications for diamond genesis and exploration. *Africa Geoscience Reviews*, **3**, 295–316.

Perk, N. W., Coogan, L. A., Karson, J. A., Klein, E. M. & Hanna, H. D. (2007). Petrology and geochemistry of primitive lower oceanic crust from Pito deep: implications for the accretion of the lower crust at the southern East Pacific rise. *Contributions to Mineralogy and Petrology*, **154**, 575–590.

Piccardo, G. B. & Guarnieri, L. (2011). Gabbro-norite cumulates from strongly depleted MORB melts in the Alpine-Apennine ophiolites. *Lithos*, **124**, 200–214.

Presnall, D. C., Dixon, S. A., Dixon, J. R., O'Donnell, T. H., Brenner, N. L., Schrock, R. L. & Dycus, D. W. (1978). Liquidus phase relations on the join diopside-forsterite-anorthite from 1 atm to 20 kbar: their bearing on the generation and crystallization of basaltic magma. *Contributions to Mineralogy and Petrology*, **66**, 203–220.

Radu, I.-B., Harris, C., Moine, B. N., Costin, G. & Cottin, J.-Y. (2019). Subduction relics in the subcontinental lithospheric mantle evidence from variation in the $\delta^{18}O$ value of eclogite xenoliths from the Kaapvaal craton. *Contributions to Mineralogy and Petrology*, **174**, 19.

Regier, M. E., Mišković, A., Ickert, R. B., Pearson, D. G., Stachel, T., Stern, R. A. & Kopylova, M. (2018). An oxygen isotope test for the origin of Archean mantle roots. *Geochemical Perspectives Letters*, **9**, 6–10.

Riches, A. J. V., Ickert, R. B., Pearson, D. G., Stern, R. A., Jackson, S. E., Ishikawa, A., Kjarsgaard, B. A. & Gurney, J. J. (2016). In situ oxygen-isotope, major-, and trace-element constraints on the metasomatic modification and crustal origin of a diamondiferous eclogite from Roberts Victor, Kaapvaal craton. *Geochimica et Cosmochimica Acta*, **174**, 345–359.

Schmickler, B., Jacob, D. E. & Foley, S. F. (2004). Eclogite xenoliths from the Kuruman kimberlites, South Africa: geochemical fingerprinting of deep subduction and cumulate processes. *Lithos*, **75**, 173–207.

Schmitz, M. D., Bowring, S. A., de Wit, M. J. & Gartz, V. (2004). Subduction and terrane collision stabilize the western Kaapvaal craton tectosphere 2.9 billion years ago. *Earth and Planetary Science Letters*, **222**, 363–376.

Schulze, D. J. (1989). Constraints on the abundance of eclogite in the upper mantle. *Journal of Geophysical Research*, **94**, 4205–4212.

Schulze, D. J., Valley, J. W. & Spicuzza, M. J. (2000). Coesite eclogites from the Roberts Victor kimberlite, South Africa. *Lithos*, **54**, 23–32.

Sharp, Z. D. (1990). A laser-based microanalytical method for the in situ determination of oxygen isotope ratios of silicates and oxides. *Geochimica et Cosmochimica Acta*, **54**, 1353–1357.

Shirey, S. B. & Richardson, S. H. (2011). Start of the Wilson cycle at 3 Ga shown by diamonds from subcontinental mantle. *Science*, **333**, 434–436.

Shirey, S. B., Richardson, S. H. & Harris, J. W. (2004). Integrated models of diamond formation and craton evolution. *Lithos*, **77**, 923–944.

Shu, Q., Brey, G. P., Hoefer, H. E., Zhao, Z. & Pearson, D. G. (2016). Kyanite/corundum eclogites from the Kaapvaal craton: subducted troctolites and layered gabbros from the mid- to early Archean. *Contributions to Mineralogy and Petrology*, **171**, 11–34.

Shu, Q., Brey, G. P. & Pearson, D. G. (2018). Eclogites and garnet pyroxenites from Kimberley, Kaapvaal craton, South Africa: their diverse origins and complex metasomatic signatures. *Mineralogy and Petrology* (Suppl 1), **112**, S43–S56.

Smart, K. A., Cartigny, P., Tappe, S., O'Brien, H. & Klemme, S. (2017a). Lithospheric diamond formation as a consequence of methane-rich volatile flooding: an example from diamondiferous eclogite xenoliths of the Karelian craton (Finland). *Geochimica et Cosmochimica Acta*, **206**, 312–342.

Smart, K. A., Tappe, S., Simonetti, A., Simonetti, S. S., Woodland, A. B. & Harris, C. (2017b). Tectonic significance and redox state of Paleoproterozoic eclogite and pyroxenite components in the slave cratonic mantle lithosphere, voyageur kimberlite, Arctic Canada. *Chemical Geology*, **455**, 98–119.

Smyth, J. R., Caporuscio, F. A. & McCormick, T. C. (1989). Mantle eclogites: evidence of igneous fractionation in the mantle. *Earth and Planetary Science Letters*, **93**, 133–141.

Sommer, H., Jacob, D. E., Stern, R. A., Petts, D., Mattey, D. P. & Pearson, D. G. (2017). Fluid-induced transition from banded kyanite- to bimineralic eclogite and implications for the evolution of cratons. *Geochimica et Cosmochimica Acta*, **207**, 19–42.

Stachel, T., Aulbach, S., Brey, G. P., Harris, J. W., Leost, I., Tappert, R. & Viljoen, K. S. (2004). The trace element composition of silicate inclusions in diamonds: a review. *Lithos*, **77**, 1–19.

Stakes, D. S. & Taylor, H. P. (1992). The northern Samail ophiolite: an oxygen isotope, microprobe, and field study. *Journal of Geophysical Research*, **97**, 7043–7080.

Sun, S.-s & McDonough, W. F. (1989) Chemical and isotopic systematics of oceanic basalts: implications for mantle composition and processes. In: (Saunders A. D. & Norr M. N. (eds)) *Magmatism in the Ocean Basins, Geological Society Special Publication*, Vol. **42**, pp. 313–345.

Viljoen, K. S., Schulze, D. J. & Quadling, A. G. (2005). Contrasting group I and group II eclogite xenolith petrogenesis: Petrological, trace element and isotopic evidence from eclogite, garnet-websterite and alkremite xenoliths in the Kaalvallei kimberlite, South Africa. *Journal of Petrology*, **46**, 2059–2090.

Warren, J. M. (2016). Global variations in abyssal peridotite compositions. *Lithos*, **248–251**, 193–219.

Weyer, S., Münker, C. & Mezger, K. (2003). Nb/ta, Zr/Hf and REE in the depleted mantle: Implications for the differentiation history of the crust-mantle system. *Earth and Planetary Science Letters*, **205**, 309–324.

Windley, B. F., Kusky, T. & Polat, A. (2021). Onset of plate tectonics by the Eoarchean. *Precambrian Research*, **352**, 105980–106022.

Workman, R. K. & Hart, S. R. (2005). Major and trace element composition of the depleted MORB mantle (DMM). *Earth and Planetary Science Letters*, **231**, 53–72.